NASA Technical Paper 1613

Experimental Evaluation of a Spinning-Mode Acoustic-Treatment Design Concept for Aircraft Inlets

Laurence J. Heidelberg, Edward J. Rice,
and Leonard Homyak

APRIL 1980

NASA

NASA Technical Paper 1613

Experimental Evaluation of a Spinning-Mode Acoustic-Treatment Design Concept for Aircraft Inlets

Laurence J. Heidelberg, Edward J. Rice,
and Leonard Homyak
Lewis Research Center
Cleveland, Ohio

National Aeronautics
and Space Administration

**Scientific and Technical
Information Office**

1980

Summary

An aircraft-inlet suppressor design method was qualitatively checked by testing a series of liners on a YF-102 turbofan engine. The design method is based on the theoretically derived result that mode cutoff ratio correlates the optimum wall impedance, the maximum possible attenuation for a mode, and its far-field radiation pattern. Most of the test liners were designed for the blade passing frequency (BPF), but two were designed for the multiple pure tones (MPT's). Far-field directivity of the BPF tone was used extensively to evaluate the results since the radiation angle can be related to the cutoff ratio.

In most cases the observed changes in the BPF directivity were consistent with the theory and assumptions used in the liner design. Liners designed for near-cutoff modes were generally more effective than ones designed for more-cuton modes. This was expected since theoretical results indicated that near-cutoff modes have a higher potential for suppression and that there are potentially a greater number of them present. The best of the BPF liners attained a suppression at design frequency of 19 decibels per unit length-diameter ratio L/D. The best MPT liner attained a remarkable suppression of 65.6 decibels per unit L/D. These attenuations may be only part of the maximum possible attenuation since the effect of boundary-layer thickness on wall resistance was neglected in the liner designs. The resulting lower-than-planned wall acoustic resistances suggest that still higher attenuations are possible. The trends and observations of the test data lend much qualitative support to a design method based on the mode cutoff ratio. Although this design method is presently incomplete, it appears to be headed in the right direction.

Introduction

Turbofan-engine fan noise produces a spinning-mode structure while propagating within the inlet duct. These spinning modes must be considered in order to design an effective inlet suppressor (refs. 1 to 3). A design method based on the mode cutoff ratio is presented in reference 4. This method is based on the observation from theory that the mode cutoff ratio correlates the optimum wall impedance, the maximum possible attenuation for a mode, and its far-field radiation pattern. A series of acoustic liners were designed and built to provide a qualitative test of this design philosophy. These liners were tested on an Avco Lycoming YF-102 turbofan engine at the NASA Lewis Research Center. This report describes these tests and presents their results. The test liners were not designed to provide balanced overall engine inlet suppression but used the engine as a research tool.

Seven of the liners were built to suppress the blade-passing-frequency (BPF) noise of the fan. Two other liners were designed and built by the same methods to suppress multiple pure tones (MPT's). The liners were tested individually and in combination. One of the combinations tested employed three liners, each designed for a progressively higher cutoff ratio. Far-field acoustic measurements were made to evaluate the liners and to gain insight into attenuation, propagation, and modal energy distribution of fan inlet noise. Far-field directivity of the BPF tone was used extensively to evaluate the results since the far-field radiation angle can be related to the cutoff ratio (ref. 5).

Spinning-mode sound propagation theory predicts that the optimum acoustic impedance for the attenuation of well-cuton modes (high cutoff ratio) is a strong function of the boundary-layer thickness of the inlet flow over the liner. In an attempt to verify this part of the theory, the boundary-layer thickness was changed. Some of the inlet flow near the wall was bled off in order to reduce the boundary-layer thickness. Boundary-layer thickness was increased for a particular liner by moving the liner downstream, or closer to the fan. The results of these boundary-layer changes are also reported herein.

Symbols

b	backing depth of liner, m
d_0	hole diameter of liner face sheet, m
c	speed of sound, m/sec
D	duct diameter, m
$\mathfrak{D}$	modal density function
ΔdB	sound power attenuation, dB
$(\Delta dB)_m$	maximum possible sound power attenuation, dB
f	frequency, Hz

i	$\sqrt{-1}$
L	acoustic liner length, m
M_0	axial steady-flow Mach number, free-stream uniform value
m	spinning-mode lobe number (circumferential order)
N_F	fan speed, rpm
n	exponent of modal power biasing function (ref. 5)
P_m	far-field acoustic pressure amplitude due to multimodal summation of principal lobes, N/m^2
R	amplitude of eigenvalue α
r_0	circular duct radius, m
t	mass reactance effective length, m
α	complex radial eigenvalue ($\alpha = Re^{i\phi}$)
δ	boundary-layer thickness, m
δ	boundary-layer displacement thickness, m
η	frequency parameter, fD/c
θ	specific acoustic resistance
μ	radial mode number
ξ	cutoff ratio
ξ_{hw}	cutoff ratio in hard-wall duct
σ	liner open-area ratio
Φ	far-field angle measured from inlet centerline, deg
Φ_p	Φ for peak of principal lobe, deg
ϕ	phase angle of eigenvalue, deg
χ	specific acoustic reactance
ω	circular frequency, rad/sec

Acoustic Liner Design

The acoustic liners were designed to provide a qualitative test of the design philosophy reported in references 4 and 6. No attempt was made to design a liner set that would provide maximum noise attenuation over the noise spectrum. The design method is based on the observation from theory that the mode cutoff ratio correlates the optimum wall impedance, the maximum possible attenuation for a mode, and its far-field radiation pattern. The optimum impedance calculations were made for spinning modes in a circular duct with a uniform steady flow except at the walls, where a one-seventh-power boundary-layer profile was assumed (ref. 6).

The test of the design philosophy is referred to as qualitative since the design technique is not considered to be complete at this time. Additional effects such as modal scattering at liner interfaces have not as yet been included in the procedure. Also, the distribution of acoustic power with cutoff ratio cannot be accurately determined. A first attempt has been made to obtain this power distribution from a multimodal far-field radiation pattern in reference 5, but it is anticipated that this technique will be altered to account for convective effects in the inlet duct.

The following main conclusions of references 4 to 6 are of use in the present discussion of liner design philosophy: For a given duct geometry, frequency parameter η, Mach number M_0, and ratio of boundary-layer thickness to duct radius δ/r_0, the optimum wall impedance is a function of the mode cutoff ratio only. The maximum possible attenuation can be approximately expressed as (e.g., ref. 4)

$$\frac{(\Delta dB)_m}{L/D} \approx -\frac{40}{\xi\sqrt{1 - M_0^2}} \tag{1}$$

where the cutoff ratio ξ is given by

$$\xi = \frac{\pi\eta}{R\sqrt{(1 - M_0^2)\cos 2\phi}} \tag{2}$$

Comparing this equation with the results of the exact calculations shown in figure 2 of reference 4 shows this to be an adequate representation of the maximum sound attenuation except near unity cutoff ratio, where equation (1) underpredicts the attenuation somewhat. The principal lobe of the single-mode radiation pattern has been shown to be located at (refs. 5 and 6)

$$\sin \Phi_p \approx \frac{1}{\xi_{hw}} \tag{3}$$

where ξ_{hw} is the hard-wall cutoff ratio, as distinguished from that of equation (2) which is for the soft-wall optimum. For qualitative discussion, ξ and ξ_{hw} can be considered to be equal.

Another consideration in the liner design procedure is that the modes are potentially much more numerous near cutoff. This can be seen from the modal density function

$$\mathfrak{D} \approx \frac{2}{\xi_{hw}^3} \tag{4}$$

which was introduced in reference 7.

These ideas can be combined to provide a multimodal liner design procedure. This has been reported in reference 4 but will be summarized here for completeness. This discussion can be clarified by using figure 1. A locus of optimum attenuation is first generated by using the optimum-impedance-versus-cutoff-ratio correlations of reference 8. The cutoff ratio is known for all points along this locus and is noted for five points. Only five points are shown here for illustration although in an actual liner design many more points would be used. Each of these points represents the centroid of an equal number of modes that in theory behave similarly in the liner and in the far-field radiation. The cutoff ratios for these centroids are determined from the modal density function (eq. (4)). Each group of modes will have a radiation pattern in the far-field, in which the peak of the principal lobe is located according to equation (3). These angles are noted on figure 1. A more complete description of the radiation pattern as a function of cutoff ratio, as found in reference 5, must be used for actual liner calculations. The additional radiation information would contain principal-lobe widths and also side-lobe contributions.

Next consider an arbitrary wall impedance, as shown by the square symbol in figure 1. The damping of each of the five modal groups must be calculated for this wall impedance. Since this point does not coincide with any of the points on the optimum locus, equation (1) does not apply directly. An off-optimum correction must be applied by using the approximate method of reference 9. In general, the further the actual wall impedance is away from the optimum impedance of a particular modal group, the greater the reduction from equation (1) will be for this modal group. When the off-optimum attenuation of each modal group is established, a correction for end reflection is made (ref. 5) and the far-field radiation pattern is established by adding up the contributions of all the modal groups. The hard- and soft-wall radiation patterns are compared and the attenuation directivity thus is established. In all this we are assuming that the acoustic power in each modal group can be established. Each group will contain equal acoustic power if equal power per mode is assumed.

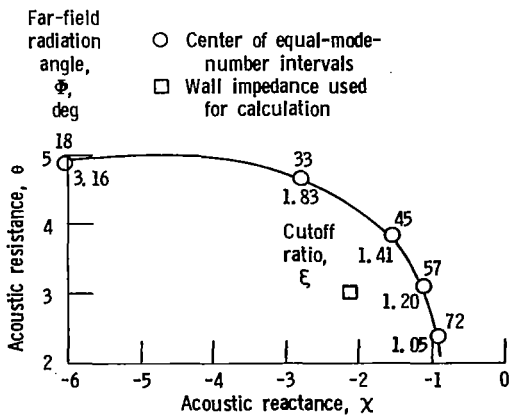

Figure 1. - Optimum impedance locus with equal-mode-number intervals.

In summary, the attenuation of sound in the duct and the consequent radiation to the far-field are predominantly determined by the mode cutoff ratio. Modes with similar cutoff ratios can be assumed to behave similarly regarding suppression and radiation. Additionally, reference 5 has shown that the cutoff ratio also controls the duct-end reflection. These approximations provided the basis for the selection of the inlet liners that were tested in the present program.

Specification of Acoustic Liners

Loci of optimum impedances for several spinning modes and three boundary-layer thicknesses are shown in figure 2(a). The modes represent samples of all the propagating modes ($\xi \geq 1$); the boundary-layer thicknesses were estimated from the one-seventh-power, flat-plate boundary-layer theory (ref. 10) for three locations corresponding to the middle of each section. The flow conditions were those that were anticipated for the YF-102 engine at full power, and the frequency was the blade passing frequency. Note that for a given boundary-layer thickness the optimum impedances fall along a common line. Modes with similar cutoff ratios fall together on this line. Well-propagating modes (large ξ) fall toward the lower left end of the locus; near-cutoff modes fall toward the right end of the locus.

The three liners (shown as large circles) located at a specific acoustic reactance ($\chi = -1$) represent liners designed to be near the optimum impedance of the near-cutoff modes ($\xi \approx 1$). Equation (1) implies that large attenuations are to be expected for these modes, and equation (3) shows that this attenuation should occur near the sideline since this is where the principal lobe of the near-cutoff modes propagates. Three liners were built with different resistances because of the uncertainty involved in the resistance specification. These three liners were designated B3, B4, and B5. Each liner had a length-diameter ratio L/D of 0.5.

Two liners are shown at $\chi = -2$ (large squares). The liner with the larger resistance, designated B2, was intended to be optimized for moderate-cutoff-ratio modes. Equations (1) and (3) indicate that these

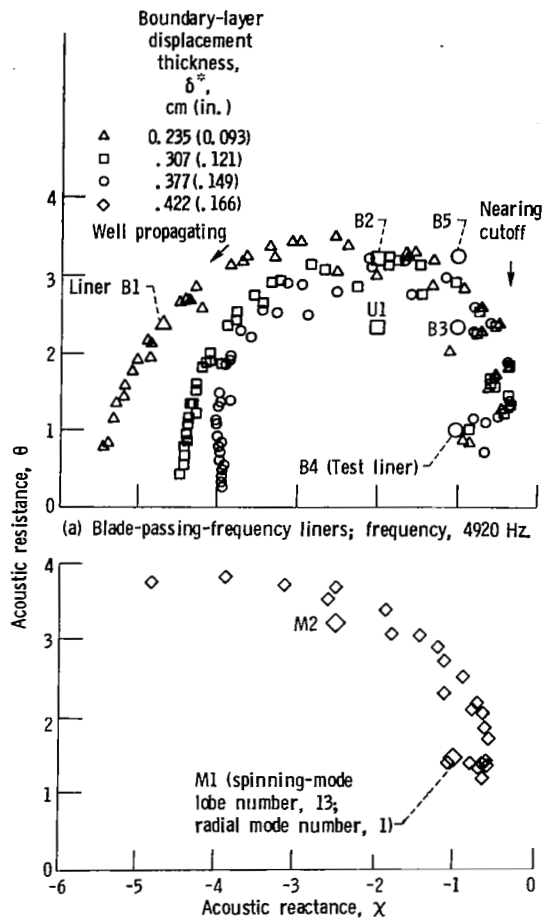

Figure 2. - Impedance optimums and test liner impedance for design conditions in YF-102 inlet. Free-stream Mach number, -0.39.

modes would be attenuated less and that this attenuation would occur closer to the axis for liner B2 than for liners B3, B4, and B5. The lower resistance liner, designated U1, was designed to be a good reference liner, with two sections being used (L/D = 1.0). The impedance of this liner is located relative to the optimum locus in a manner similar to that of previously tested well-performing liners. Liner U1 might also be considered as a lower resistance version of liner B2 for modes with moderate cutoff ratios.

Liner B1, at $\chi = -4.7$ (large triangle), was designed to be near the optimum impedance for modes with large cutoff ratios ($\xi >> 1$). Again, equations (1) and (3) show that only small attenuations of these modes can be anticipated and that these attenuations should occur nearer to the inlet axis than for the other liners.

Liners B1, B2, and B3 were intended to be run together by means of successive untaping of the liners. The logic used to specify these liners originated in thinking about single modes. In a static test, a multitude of modes can be anticipated. The presence of many modes complicates the interpretation of actual data. Although liner B1 was optimized for well-propagating modes, it will also heavily attenuate the near-cutoff modes because these modes are easily attenuated even by off-optimum liners. Thus, to test the notions expressed by equations (1) and (3), the liners had to be activated in a particular order. Liner B3 had to be untaped, or activated, first so that the easily attenuated near-cutoff modes were removed first. Liner B2 was then exposed and the increment in attenuation observed. Finally, liner B1 was untaped and again the increment in attenuation was analyzed.

The locus of optimum impedance for conditions at the anticipated peak in the multiple-pure-tone spectrum is shown in figure 2(b). Several propagating modes are shown. The most likely mode involved in this noise source is the first radial mode of the thirteen-lobed pattern ($m = 13$; $\mu = 1$). The dominance of this mode assumes that the mode is locked to the rotor rotation and that the frequency is thus correct for this mode. The liner designed for this mode, which is also near cutoff, was thus the primary liner and was designated liner M1. The secondary liner, which was aimed at higher cutoff ratios, was designated M2. Each of these liners could be tested individually with the previously described blade-passing-frequency liners (B1 to B5).

Models of the acoustic resistance and reactance were used in figure 2. The resistance model used was the grazing flow component (amplitude effect neglected) of equations developed in reference 11.

$$\theta = \frac{0.3\ M_0}{\sigma} \tag{5}$$

The effect of boundary-layer thickness on the resistance was ignored since reference 12 indicated that the resistance varied only as the one-tenth power of boundary-layer thickness. In retrospect, this was seen to be a mistake, as will be shown in the next section. The reactance model used was (ref. 13)

$$\chi = \frac{\omega t}{\sigma c} - \cot \frac{\omega b}{c} \tag{6}$$

The effective length t was assumed to be equal to the perforated-plate thickness. This assumption is valid in the presence of grazing flow. The resultant

TABLE I. – DESIGN PARAMETERS FOR ACOUSTIC LINER PANELS

[All facing sheets were 0.051-cm- (0.020-in.-) thick, perforated 2024-T3 aluminum sheet with punched holes of 0.140 cm (0.055 in.) diameter.]

Liner	Open-area ratio, σ, percent	Backing depth, b		Length diameter ratio, L/D	Design frequency Hz
		cm	in.		
B1	5.3	0.193	0.076	0.5	4920
B2	3.8	.328	.129		
B3	5.3	.531	.209		
B4	11.2	.688	.271		
B5	3.8	.457	.180		
U1	5.3	.363	.143		
M1	8.0	2.377	.936	.25	1600
M2	3.8	1.123	.442	.25	1600

parameters for the acoustic liners are shown in table I.

Evaluation of Liner Properties by Using Measured Flow Conditions

Several changes have occurred since the liners for these tests were originally designed. As discussed in the "Test Procedure" section of this report the full-speed condition could not be attained, although this was one of the more minor problems. A more serious problem was that the boundary layers were thicker than anticipated, and their effect on the acoustic impedance has been reassessed.

As mentioned in the previous section, the effect of boundary-layer thickness on the acoustic resistance of the perforated plate was ignored because of the test results of reference 12. Other studies, such as that described in reference 14, include the effects of boundary-layer thickness on acoustic resistance in a fairly complicated empirical model. Both references 12 and 14 were based on the steady flow resistance of perforated plates. Consideration of some new acoustic resistance measurements (ref. 15) showed that boundary-layer thickness can have a considerable effect on the acoustic resistance of perforated plates. These data were used in combination with the theoretical results of reference 16 to generate a new model for the acoustic resistance, which is

$$\theta = \frac{M_0}{\sigma\left(2 + 1.256\,\frac{\delta^*}{d_0}\right)} \qquad (7)$$

In the limit when $\delta^* = 0$, equation (7) yields the theoretical results of reference 16, which assumed uniform grazing flow and thus no boundary layer. Equation (7) is also compatible with the data of reference 15.

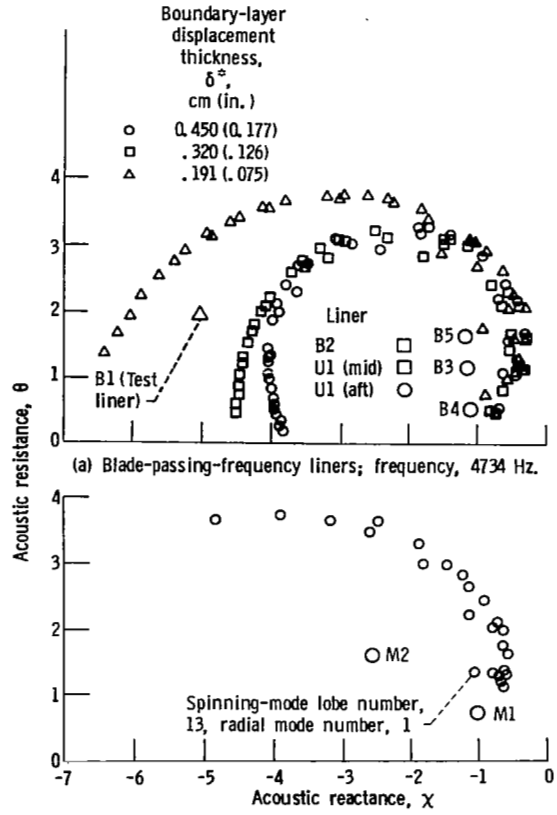

Figure 3. - Impedance optimums and test liner impedance for actual test conditions in YF-102 inlet. Free-stream Mach number, -0.38.

Figure 3 shows where the estimated liner impedances are located relative to the calculated optimum impedance loci. All the liners are now seen to be underdamped (resistance too low). Two phenomena have occurred that have changed the relative positions of the actual impedances and the optimum impedances between figures 2 and 3. The optimum-impedance loci have shifted because of a frequency shift (in the case of the BPF liner) and flow changes caused by the lower actual engine test speed. More importantly, the estimated acoustic resistances of all the liner panels have been reduced dramatically as a result of the boundary-layer thickness effect expressed in equation (7). Thus the tests would have been more conclusive if the open-area ratios had been reduced for the liners shown in table I to give higher resistance values. In the case of the MPT liners, M2

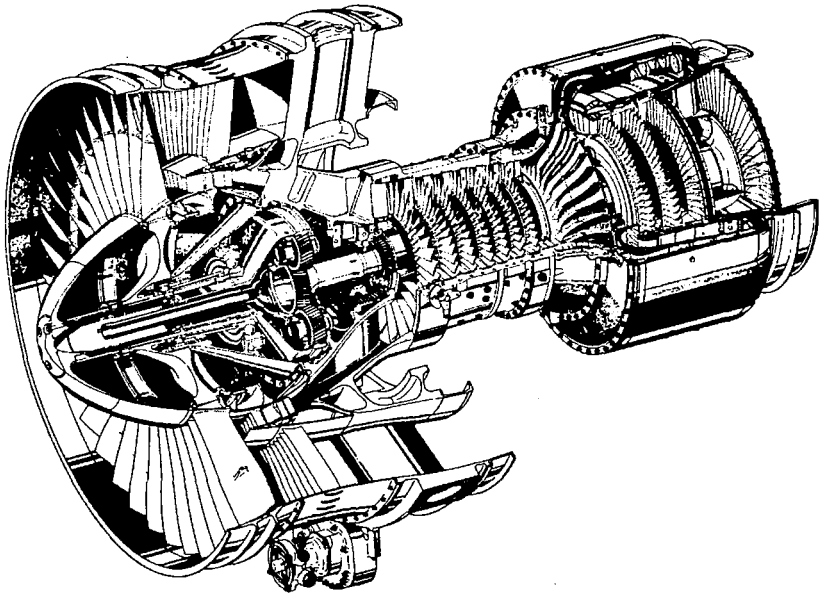

Figure 4. - Cutaway view of YF-102 turbofan engine.

has moved a significant distance from the optimum impedance locus, but M1 is still fairly close to the optimum locus.

Apparatus and Procedure

Engine

The engine used in this investigation was an Avco Lycoming YF-102. This twin-spool turbofan engine has a bypass ratio of 6, a fan pressure ratio of 1.47, a fan tip Mach number of 1.2, and a maximum rated thrust of 33 kilonewtons (7500 lb). Figure 4 shows a cutaway view of the YF-102 engine. The engine core consists of a combination seven-stage axial, single-stage centrifugal compressor driven by a two-stage axial turbine and an external atomizing combustor. The front fan and one supercharging stage are gear driven by a two-stage coaxial power turbine. The fan has 40 blades and is 1.02 meters (40 in.) in diameter. There are 85 fan-bypass stator vanes and 84 fan-core stator vanes. The blade-vane ratios for this fan lead to a cutoff rotor-stator interaction tone for the BPF. Table II shows some of the engine performance and inlet parameters of interest at the three fan speeds used in this investigation.

A very long test inlet was used in this investigation. The total length-diameter ratio L/D was 3.6. A schematic diagram of the inlet assembly showing its various sections is presented in figure 5. The flow entered a large-radius bellmouth, where it was lead into the first of many constant-diameter sections. This first section was used to measure the inlet total flow rate. Next the flow entered a short section that was used to bleed off the boundary-layer flow. This section had a perforated wall of 20 percent open area. The cavity behind the perforated wall was connected to six suction hoses, which were in turn connected to an air ejector. With this system the boundary-layer thickness could be reduced by a factor of up to 5, depending on the inlet flow rate. When bleed was not used, the perforated wall of this section

TABLE II. – YF-102 ENGINE AND INLET PERFORMANCE AT SEA-LEVEL-STATIC, STANDARD-DAY CONDITIONS

	Test fan speed, rpm		
	7100	5900	4500
Thrust, kN (lb)	31.1 (7000)	20.2 (4550)	11.1 (2500)
Core speed, rpm	18 900	17 600	15 800
Fan bypass pressure ratio	1.44	1.28	1.15
Total fan airflow, kg/sec (lb/sec)	118.8 (262.0)	97.3 (214.5)	73.7 (162.5)
Inlet duct Mach number	0.375	0.298	0.221
Fan tip relative Mach number	1.25	1.02	0.765
Blade passing frequency, Hz	4733	3933	3000

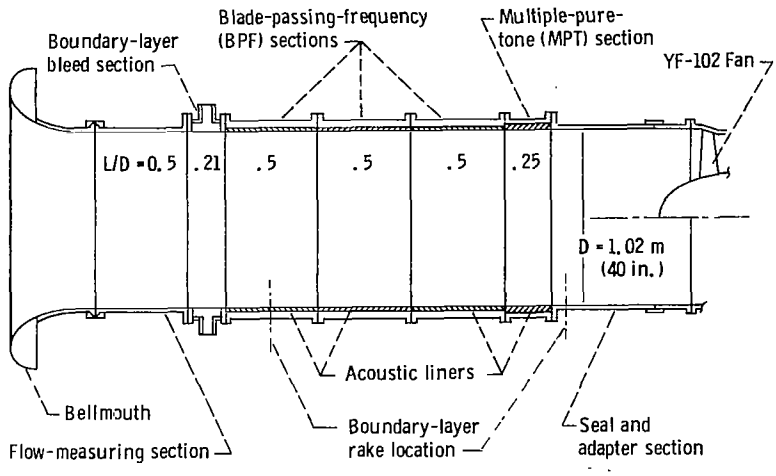

Figure 5. - Inlet assembly with replaceable acoustic liners.

was covered with aluminum tape. Details of the design and performance of this bleed system are presented in reference 17.

The next three sections of the inlet were used to mount the acoustic liners designed to remove the BPF tone. Each section had an L/D of 0.5 and was capable of holding any one of the BPF liners. The first BPF section had provisions for mounting a boundary-layer rake on the wall half-way between the end flanges. The MPT section was connected downstream of the last BPF section. The L/D of the MPT section was 0.25.

The last section was an inlet seal and engine adapter. A second boundary-layer rake was mounted in this section just downstream of the acoustic liners.

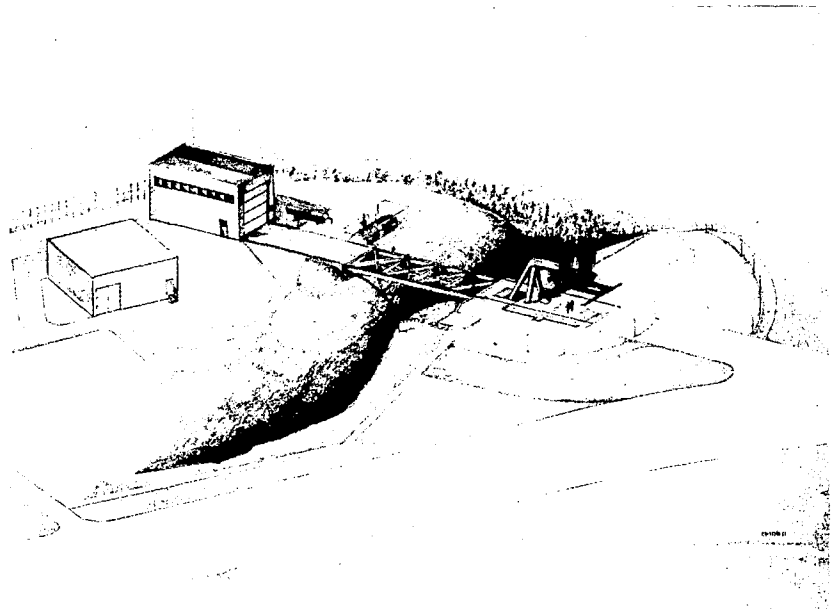

Figure 6. - Perspective view of NASA Lewis fan-noise test facility.

Test Facility

The Lewis outdoor test facility for noise and performance testing accommodates turbofan engines with thrust levels to 133 500 newtons (30 000 lb). A perspective sketch of this facility is shown in figure 6. The test engine is supported by a tripodded, cantilevered, overhead support arm. This support arm contains a thrust-measuring mount to secure the engine 2.9 meters (9.5 ft) above the ground plane. A movable shelter, on tracks, covers and protects the engine between test runs.

Engine instrument and control liners run to a vault next to the test stand. Conditioned signals are transmitted from the vault to the operation control room. The control room, located approximately 120 meters (400 ft) from the engine, contains equipment to control engine operation and to receive all engine transducer signals. A digital data acquisition system, together with a computer system, provides on-line engine performance data.

Aft-radiated engine noise, as well as jet noise, is effectively eliminated by a large exhaust muffler. Figure 7 depicts the engine on the test stand with its exhaust ducted to the muffler. A nozzle at the entrance to the muffler is sized to provide fan operating conditions (flow and pressure ratio) nearly identical to those before the muffler was connected. This muffler is 18.3 meters (60 ft) long and has an inside diameter of 1.68 meters (66 in.). The muffler is lined with a 59-centimeter- (23.3-in.-) deep bulk absorber.

Acoustic Instrumentation and Processing

The acoustic arena is a 30.5-meter- (100-ft-) radius, concrete surface centered on the engine inlet. There are 12 ground microphones on the perimeter of the arena. They are positioned at 10-degree intervals from 10° to 120°, measured from the engine inlet axis. Each 1.3-centimeter- (0.5-in.-) diameter microphone is mounted on 0.6-meter- (2-ft-) square composition hardboard at ground level and pointed at the inlet.

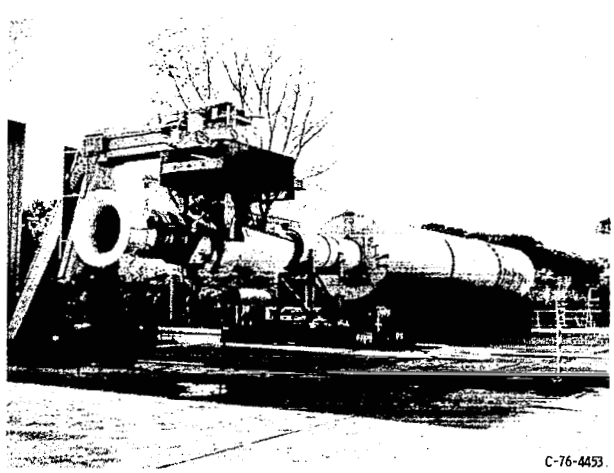

Figure 7. - YF-102 engine on test stand with exhaust muffler.

The microphone signals, transmitted over shielded cable to amplifiers, are conditioned by gain settings for frequency-modulated (FM) magnetic tape recording. The conditioned signals are recorded on a 16- to 20-second-duration tape loop. This acoustic system is calibrated, from the microphones through the amplifiers, with a pistonphone both before and after each run.

The tape loop was replayed and analyzed through a Novatronic scanner-control unit. The Novatronic separately plays each acoustic channel into a General Radio multifilter and multichannel rms detector. During 16 seconds of integration time, a one-third-octave-band sound pressure level (SPL) was obtained. Integration was performed over 1024 data samples to reduce the uncertainty of the random signal measurement. The resulting sound pressure levels, in units of decibels (dB), were referenced to 2×10^{-5} pascal (0.0002 microbar). The resulting sound power levels were referenced to 10^{-13} watt. All further data were processed on an IBM-TSS 360 computer.

The IBM computer calculates sound levels, at locations other than the measured stations, as described in reference 18. All data were corrected to an atmospheric temperature of 15° C (59° F) and a relative humidity of 70 percent. Ground microphone data were corrected to free-field conditions by subtracting 6 decibels at all frequencies to 20 000 hertz. This correction accounts for the effect of ground-reflected signals. Theory predicts a 6-decibel correction for a perfect reflecting surface. Tests of the acoustic arena have indicated that the correction is approximately 6 decibels.

Test Procedure

The engine was run at three fan speeds; 4500, 5900, and 7100 rpm. Physical rather than corrected fan speed was used to keep the BPF tone in a single one-third-octave band from one test day to another. It was originally planed to run the engine at 7380 rpm, the design speed for the BPF liners. Unfortunately, this speed could not be achieved when the ambient temperature was high. A speed of 7100 rpm was chosen in place of 7380 rpm because it was the highest speed that could be reached during the highest ambient temperatures that were likely to occur. All tests were run after 6 p.m. when the wind speed was under 16 km/hr (10 mph). The 7100-rpm speed was repeated twice for each configuration and the data were averaged.

The baseline, hard-wall data were taken at the beginning of each evening's run. All configurations tested in that run were then compared with that baseline in order to obtain suppression data (differences) of high accuracy. The differences in the baseline BPF levels from one run to the next were generally within ±2 decibels, but the repeatability of the BPF during an individual run was usually ±0.5 decibel.

Aluminum adhesive tape was used to cover the acoustic liners that were not part of the configuration being tested. Thus, by removing tape and sometimes by adding tape, several configurations could be tested in a run.

Results and Discussion

The YF-102 engine was used to test several acoustic liners and liner combinations in the inlet. These liners were designed specifically to operate on the spinning modes of the BPF tone and the MPT's. All testing was done with the engine exhaust ducted to a large muffler in order to measure only inlet noise. All the data are presented on a one-third-octave-band basis. Narrow-band analysis was performed on a number of representative data samples. These narrow-band spectra show the BPF tone to be sufficiently strong to be accurately represented by the one-third-octave band the tone falls within. The data have been adjusted to free-field and standard-day conditions. The baseline or hard-wall data presented are an average of 11 runs, each taken on a different evening over a period of several months. Three fan speeds (7100, 5900, and 4500 rpm) were run for each configuration.

Unsuppressed Engine Noise

The inlet power spectra at the three test fan speeds is shown in figure 8. At a fan speed of 7100 rpm the blade-tip relative Mach number was supersonic and the characteristic MPT's were very much in evidence. These MPT's peaked at 1600 hertz and were only about 2 decibels below the BPF tone at 5000 hertz. At the two lower fan speeds (5900 and 4500 rpm) there was an absence of MPT's, and the BPF and its harmonics dominated the power spectra. At very low frequencies (<400 Hz), noise originating from within the muffler and exhaust system contributed significantly to the power spectrum. Most of this low-frequency noise propagated upstream through the fan nozzle, aft fan duct, and fan and then out the inlet.

The far-field directivity of the BPF tone has been shown to be related to the modal structure at the upstream end of the inlet duct. An analytical method

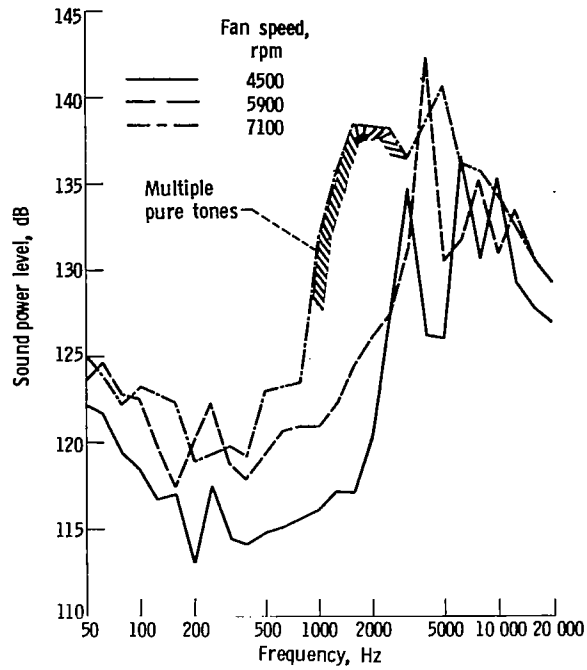

Figure 8. - YF-102 unsuppressed-inlet power spectra - averaged data, front quadrant.

has been developed in reference 5 that determines the acoustic power produced by a fan, as a function of the mode cutoff ratio, from the far-field radiation pattern. It is helpful in interpreting the data from this investigation to use the concept that far-field directivity is a function of acoustic power versus mode cutoff ratio. Figure 9 shows the directivity of the BPF tone at the three test speeds. The dashed line on these plots is an attempt to fit a modal energy distribution to the data by using the equations of reference 5. The exponent n altered the acoustic power distribution as a function of the cutoff ratio. Equal energy per mode is represented by an exponent of 0. An exponent of 1 shifted the power toward the lower cutoff ratios (near cutoff and propagating away from the inlet axis). At the highest fan speed the directivity was best matched by an equal energy per mode plus the rotor-locked mode. The rotor-locked mode was added since the tip relative Mach number was 1.25, and thus this mode would be cut on. The lowest speed (4500 rpm) pattern also seemed to be fit by equal energy per mode. At 5900 rpm the directivity pattern was different. The energy distribution represented by n = 1 seemed to fit the data better, an indication of more energy near cutoff. Another interesting observation at 5900 rpm is that the BPF levels were higher than at any other speed.

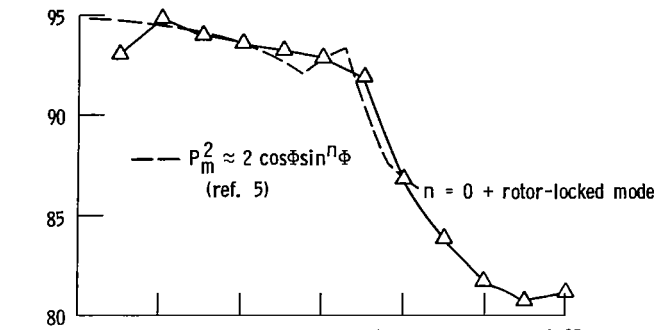

(a) Fan speed, 7100 rpm; tip relative Mach number, 1.25; frequency band, 5000 Hz.

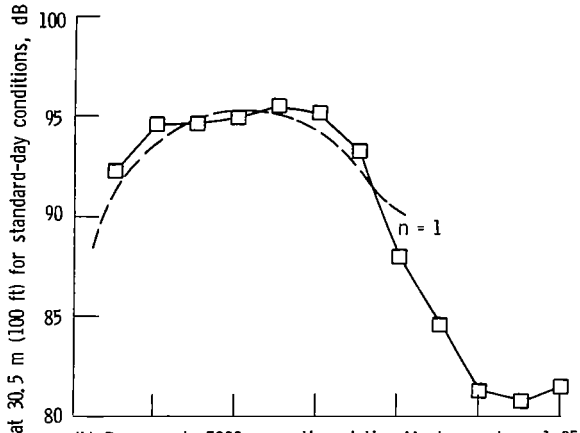

(b) Fan speed, 5900 rpm; tip relative Mach number, 1.05; frequency band, 4000 Hz.

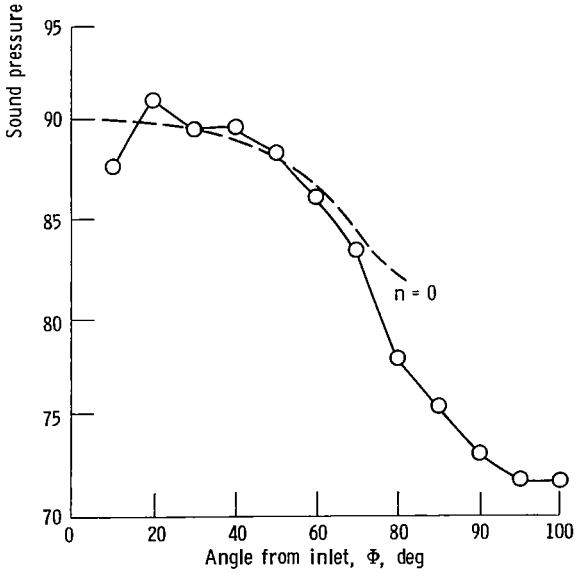

(c) Fan speed, 4500 rpm; tip relative Mach number; 0.80; frequency band, 3150 Hz.

Figure 9. - Directivity of the blade-passing-frequency tone for unsuppressed YF-102 engine.

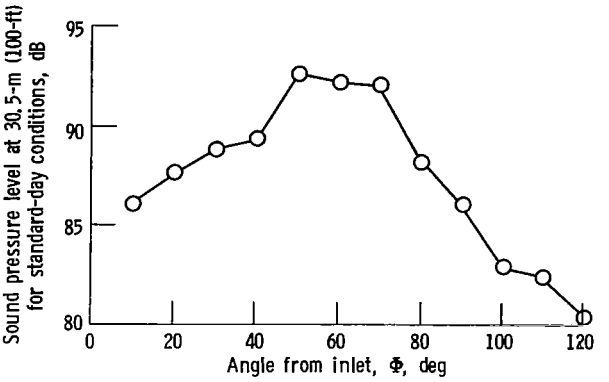

Figure 10. - Directivity of multiple pure tones. Frequency, 1600 Hz; fan speed, 7100 rpm.

Although the blade passing frequency was the most important frequency in this investigation, two acoustic liners were designed to remove the multiple pure tones. The design frequency for these liners and the peak of the MPT spectrum was 1600 hertz. The directivity pattern for this band is plotted in figure 10. Most of the energy seems to be directed toward the angles between 50° and 70°. This is typical of MPT's and indicates that most of the modes present were near cutoff.

Progressive Untaping of Liners B3, B2, B1, and MI

In this test, each of the three BPF liners was designed to have optimum impedance at three different and progressively higher cutoff ratios. These cutoff ratios correspond to near-cutoff modes, a middle region, and well-cuton modes. First the near-cutoff liner, B3, was untaped (made active). Then the middle liner, B2, was untaped; and finally the well-cuton liner, B1, was untaped - for a total of three active liners. The MPT liner, M1, designed for near-cutoff modes was also untaped.

Some of the results of this test at a fan speed of 7100 rpm (design speed) are shown in figure 11, where the directivity and suppression of the BPF tone levels are plotted. Liner B3 showed large reductions of the tone levels, particularly at far-field angles (around 70°), which are associated with the near-cutoff modes. It is not surprising that this liner was very effective since it was specifically designed to remove the near-cutoff modes. These modes are more easily attenuated (eq. (1)) and more numerous (eq. (4)) than the well-cuton modes. When liner B2 was added to the system, the BPF suppression was less than that with liner B3 alone. The peak in the suppression curve moved forward from 70° to 60°, a

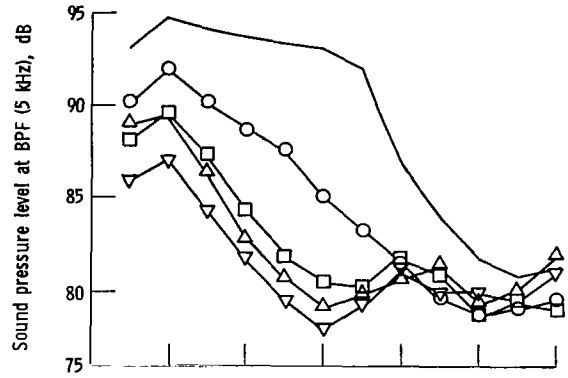

(a) Directivity at 30.5-m (100-ft) radius; standard-day conditions.

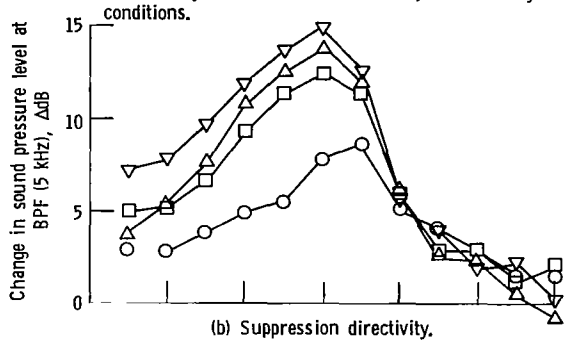

(b) Suppression directivity.

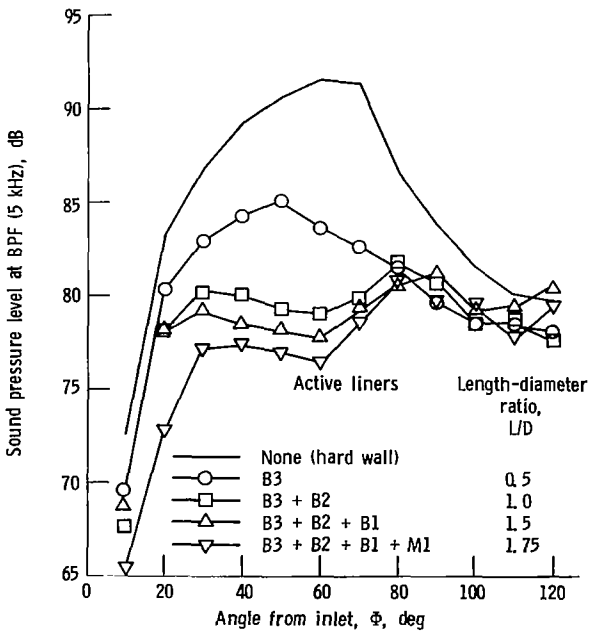

(c) Directivity at 30.5-m (100-ft) sideline; standard-day conditions.

Figure 11. - Blade-passing-frequency (BPF) directivity and suppression for progressive untaping of liners B3, B2, B1, and M1. Fan speed, 7100 rpm.

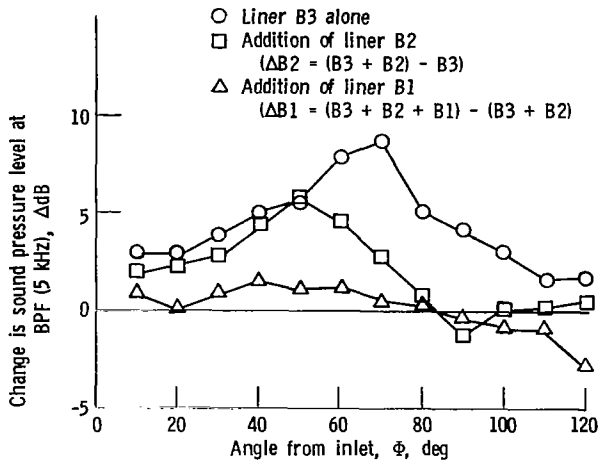

Figure 12. - Incremental blade-passing-frequency (BPF) suppression for liner combination B3 + B2 + B1. Fan speed, 7100 rpm.

possible indication of increased liner effectiveness for the more-cuton modes. Note that the sideline directivity was almost flat from 30° aft. Next, liner B1 was added and only a small increase in suppression was observed. The tone reductions with liner B1 were small, partly because it was designed to work on the well-cuton, difficult-to-attenuate modes. Finally, liner M1 was added; the small additional tone reductions achieved here were made despite the liner being designed for a frequency of one-third of the BPF and being one-half as long as the other liners. A more complete evaluation of the two MPT liners is given in the next section of this report.

To better define the contributions of each of the liners to the total system, a plot of the increase in suppression (incremental suppression) due to the addition of each liner was made. This plot is shown in figure 12 for each of the four liners. Liner B3 was most effective at 70°, near cutoff; liner B2 had a peak incremental suppression of 50°. The plot for liner B1 is very flat, but a maximum does occur at a still lower angle, 40°. Although there was a tendency for the peak in the incremental suppression directivity to move forward with increasing liner length, this effect was more pronounced in liners B3 and B2 (fig. 12) than in the uniform liners (each liner section of identical design). The results for the uniform liners are discussed later in this report. The more pronounced shift in the peak to lower angles with the addition of each liner is an indication that the liners that were added were more effective in attenuating progressively more-cuton modes. This behavior is consistent with the liner design objectives.

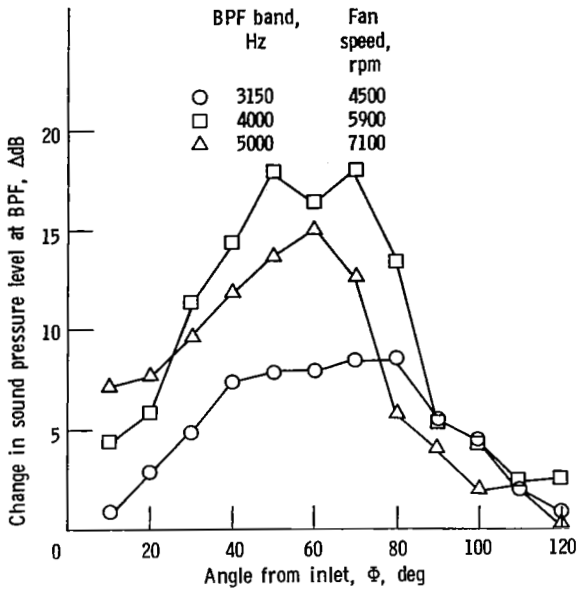

Figure 13. - Effect of fan speed on blade-passing-frequency (BPF) suppression for liner combination B3 + B2 + B1 + M1.

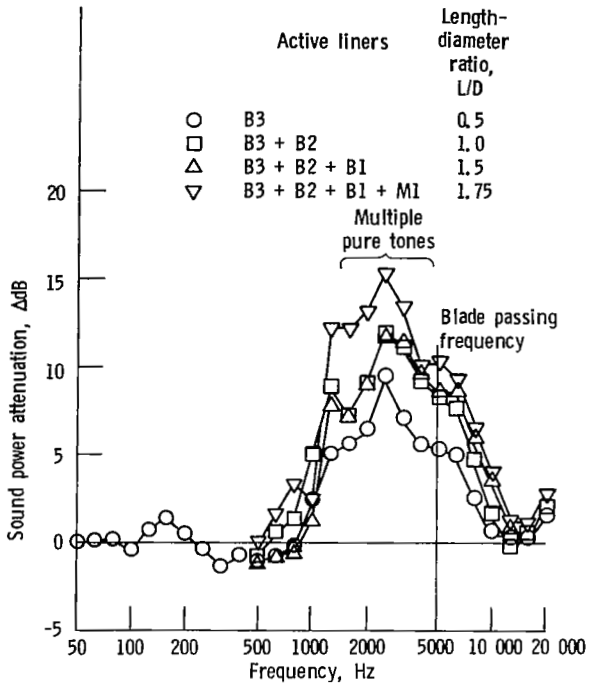

Figure 14. - Sound-power-attenuation spectra for progressive untaping of liners B3, B2, B1, and M1. Fan speed, 7100 rpm.

The effect of fan speed on the directivity of the BPF suppression for the case where all the liners were active is shown in figure 13. Although the BPF liners were designed for the 7100-rpm fan speed, the maximum BPF suppression occurred at 5900 rpm. Almost all the liners and liner combinations tested on this engine demonstrated a peak BPF suppression at a fan speed of 5900 rpm. It seems likely that this was a result of a difference in modal energy distribution between the fan at 7100 rpm and at 5900 rpm. As previously discussed (fig. 9), the fan at 5900 rpm had a modal energy distribution more heavily weighted toward the near-cutoff, more easily attenuated modes. Another indication that the fan noise at 5900 rpm for this engine was more easily attenuated comes from tests of acoustic liners with bulk treatment. These bulk treatment liners were designed by a totally difference method and in a different material, yet they all had their peak attenuations at 5900 rpm. The results of the bulk treatment liners are presented in reference 19.

The progression of sound power attenuation spectra for the four stages of suppression at 7100 rpm is shown in figure 14. Although three of the four liners were designed to remove the BPF at 5000 hertz, the peak attenuation occurred at 2500 hertz. This was due to the presence of strong and easily attenuated MPT's at this high fan speed. At the BPF, the 5000-hertz band, the first two liners to be made active were most effective in reducing the power. The next liner, B1, contributed very little. The MPT liner, M1, was in fact more effective at the BPF than was liner B1. It seemed likely that this was a result of M1 being closer to optimum impedance for near-cutoff modes than B1. Even though the three BPF liners (total L/D, 1.5) had already removed much of the power in the MPT bands, liner M1 with an L/D of only 0.25) was able to make a sizable further reduction. All the liner configurations showed a rapid drop in attenuation above 6300 hertz. The dip in attenuation just below the 20 000-hertz band may have been a result of liner self-noise. The frequency of liner self-noise was estimated from reference 20 to fall in the 16 000-hertz band at high speed and to drop with speed until it fell within the 10 000-hertz band at the lowest speed. The bandwidth of this noise should be sufficiently narrow so as to affect only a single one-third-octave band. This behavior was not fully shown in the data. Instead the dip in the spectrum moved only one band to 12 500 hertz and only at the lowest speed. Two bands seemed to be affected rather than one. Thus, it is not conclusive that the dip in the spectra was due to liner self-noise.

The effect of fan speed on the sound power attenuation spectrum for the configuration where all three BPF liners were active (system B3 + B2 + B1) is shown in figure 15. At 4500 rpm the liners' peak attenuation was at the design frequency of 5000 hertz,

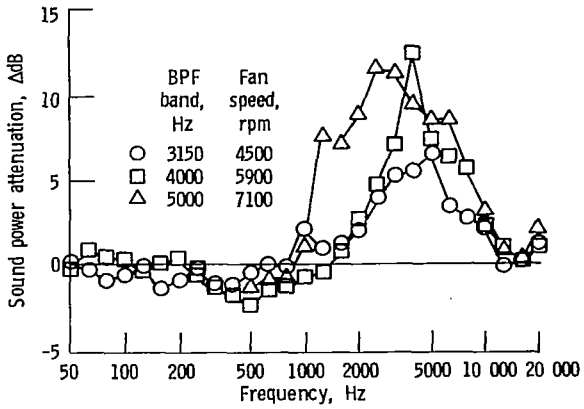

Figure 15. - Effect of fan speed on sound power attenuation for liner combination B3 + B2 + B1.

but at other speeds this effect was masked. At 5900 rpm the MPT's were absent, and this allowed the peak attenuation to occur at the BPF, in the 4000-hertzband. As previously indicated, the attenuation of the BPF at 5900 rpm was higher than that at the design speed of 7100 rpm and, as expected, higher than that at 4500 rpm.

Individual Liner Tests

In this series of tests, each of the liners used in the progressive untaping test was tested individually (i.e., as the only active liner). In addition, an MPT liner of different design was tested.

The directivity of the BPF suppression at a fan speed of 7100 rpm is plotted in figure 16 for each of the BPF liners (B1, B2, and B3). Peak suppression for all the liners occurred at 70°, or near cutoff. This might be expected since the modes near cutoff ($\xi \sim 1$) are most numerous (eq. (4)) and most easily attenuated (eq. (1)). Since liner B3 was designed to attenuate the modes near cutoff, it is not surprising that it had the highest peak suppression. Liner B1, designed for the well-cuton modes, had the lowest peak. The liner B2 peak fell between those of the other two liners. Liner B2 performed disappointingly especially at the lowest angles. Liners B3 and B1 seemed to be equally effective at the lowest angles (10° to 30°). This similarity in performance for what

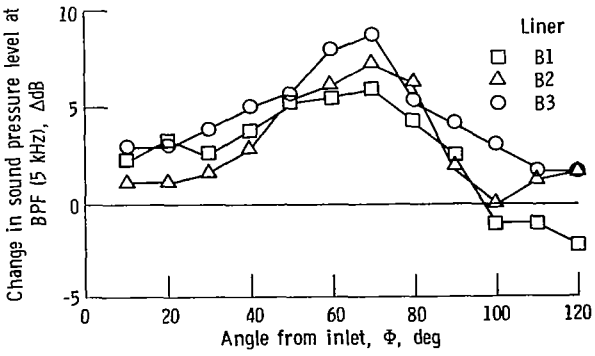

Figure 16. - Directivity of blade-passing-frequency (BPF) suppression for individual liners B1, B2, and B3. Fan speed, 7100 rpm.

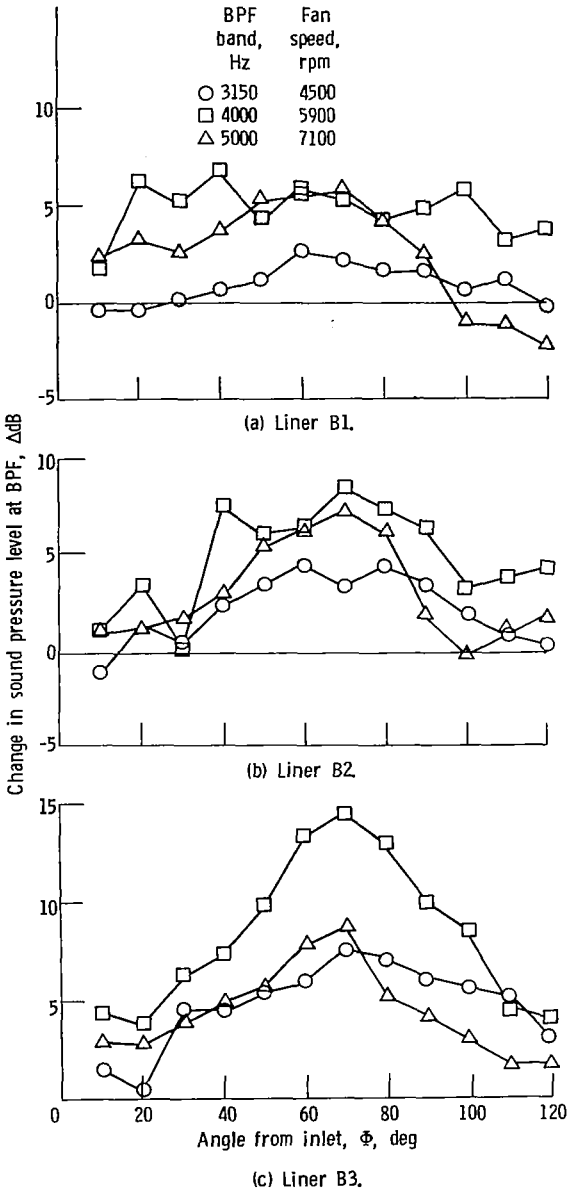

Figure 17. - Effect of fan speed on blade-passing-frequency for individual liners B1, B2, and B3.

should have been well-cuton modes was surprising in view of the design differences between liners B1 and B3. One possible reason for the poor low-angle performance of B1 relative to B3 was modal scattering between hard-wall and soft-wall sections of the inlet duct. If the modal energy distribution was changed each time a change in wall impedance was encountered, the liner may not have seen the same modal energy distribution that was present in the hard-wall case. At present, it is not known to what extent modal scattering would affect the interpretation of the data presented herein.

The performance of the three liners at the BPF for all three fan speeds is shown in figure 17. At 5900 rpm all the liners seemed to perform better individually, as they had when tested in combination. Although liner B3 showed a dramatic increase in peak BPF suppression at 5900 rpm, the other two liners showed much smaller improvements. This is consistent with the previously discussed weighting of the modal energy distribution of the fan toward cutoff at 5900 rpm. Note that at 5900 rpm, liner B1 showed a large increase in suppression at forward angles (20° to 40°) instead of at 70°, where liner B3 showed the most change. All three liners had their poorest performance at 4500 rpm.

Sound power attenuation spectra at 7100 rpm are compared for the three liners in figure 18. These spectra are dominated by MPT's, with liner B3 showing the highest attenuation of the MPT's. It is surprising to see liner B1 showing better performance for most of the MPT frequencies than liner B2. It was expected that the thicker B2 liner would be closer to optimum impedance than the thinner B1 liner at these lower frequencies. Even at the design frequency (BPF), liner B1 did slightly better than B2. Liner B3 reduced the power in the BPF band more than the other two liners, as was expected. At frequencies above the BPF the thinner liner (B1) did better than thicker liners (B2 and B3). Here the thinner liner was closer to optimum impedance for the high frequencies.

The effect of fan speed on the sound power attenuation spectrum is plotted in figure 19. Between the 1250- and 3150-hertz bands, all three liners

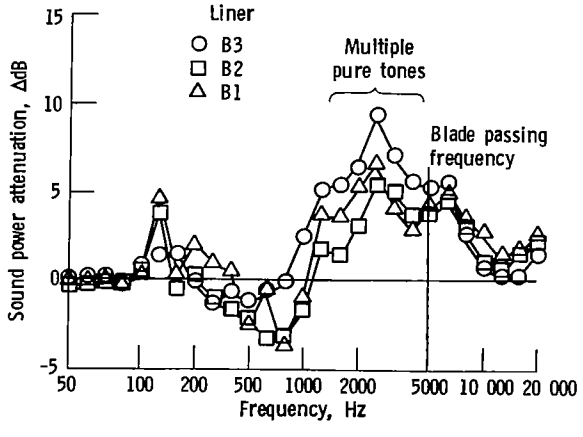

Figure 18. - Sound power attenuation for individual liners B1, B2, and B3. Fan speed, 7100 rpm.

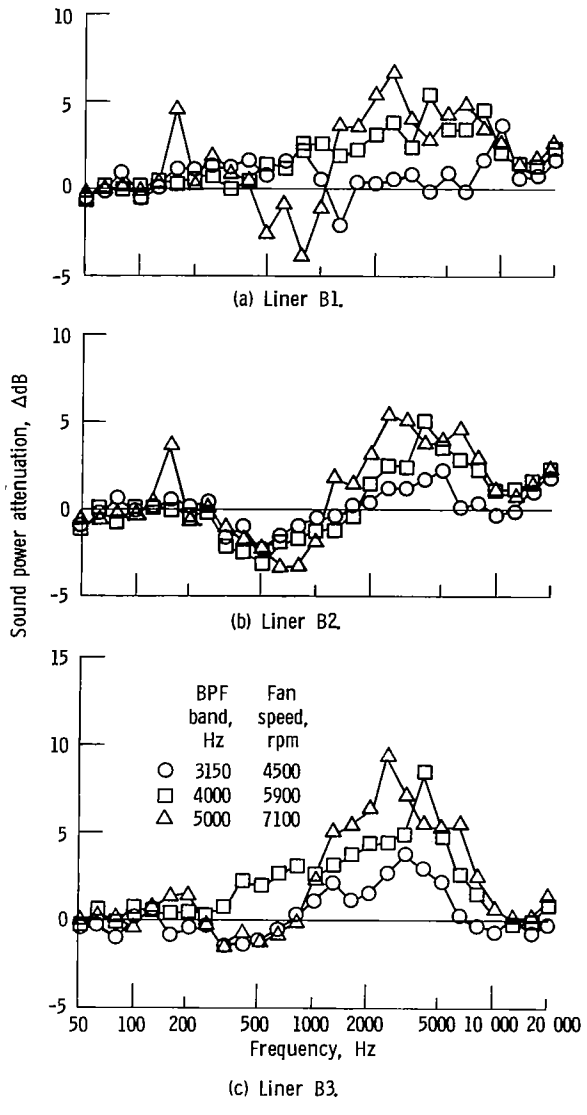

Figure 19. - Effect of fan speed on sound power attenuation spectra for individual liners B1, B2, B3.

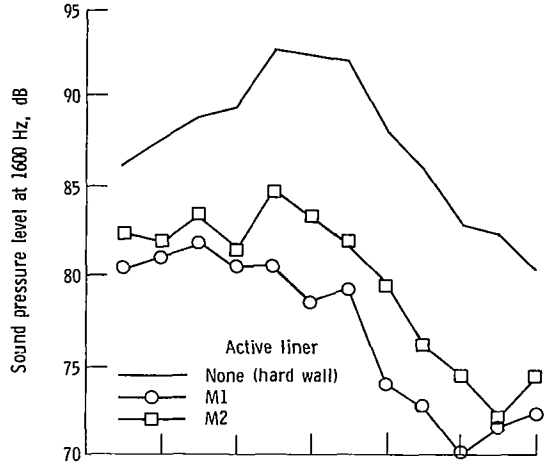

(a) Directivity at 30.5-m (100-ft) radius; standard-day conditions.

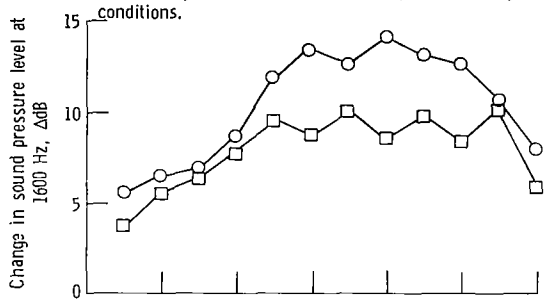

(b) Suppression directivity.

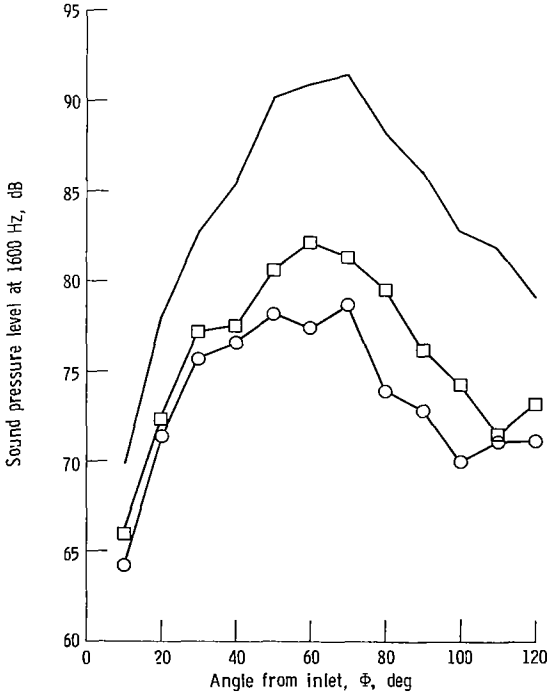

(c) Directivity at 30.5-m (100-ft) sideline; standard-day conditions.

Figure 20. - Multiple-pure-tone directivity and suppression for individual liners M1 and M2. Fan speed, 7100 rpm.

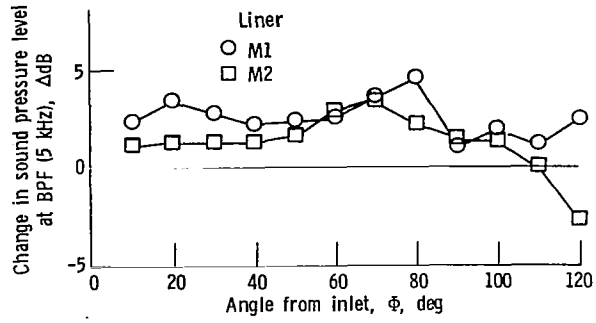

Figure 21. - Blade-passing-frequency suppression for individual liners M1 and M2. Fan speed, 7100 rpm.

showed large attenuation at 7100 rpm because of the presence of the MPT's. Although liner B1 had approximately the same performance at and above the BPF at 7100 and 5900 rpm there was almost no attenuation at 4500 rpm until the 10 000-hertz band. Liner B2 behaved similarly to B1 with speed. In addition, there was a region of negative attenuation around 500 hertz for all fan speeds. Here again, at 5900 rpm, liner B3 had higher BPF attenuation than at the design speed. As with the other liners, B3 had much lower attenuation at the lowest fan speed.

The performance of the two MPT liners, M1 and M2, is compared at their design frequency in figure 20. This figure shows the directivity of the 1600-hertz band for a fan speed of 7100 rpm at both a radius and sideline of 30.5 meters (100 ft), with the unsuppressed inlet for reference. Figure 20(b) shows the directivity of the 1600-hertz suppression. Liner M1 was designed for modes nearer cutoff than liner M2. Both liners had an L/D of only 0.25. Liner M1 showed much better performance with higher attenuations at all angles than liner M2. The peak SPL attenuation at 1600 hertz for M1 was over 14 decibels at an inlet angle of 80°, or almost 57 decibels per unit L/D. In fact, this liner produced higher SPL attenuation per unit L/D than any other liner tested at the Lewis Research Center to date. The largest SPL attenuation occurred at 2000 hertz and 70° and was 16.4 decibels, or 65.6 per unit L/D.

Liner M1 not only did an excellent job of removing the MPT's, but also was effective in removing the BPF, as shown in figure 21. On an equal-L/D basis these attenuations are comparable to those of the liners that were designed for the BPF.

The sound power attenuation spectra for both MPT liners at all three fan speeds are shown in figure 22. At 7100 rpm the liners had very high attenuation for frequencies containing the MPT's. Liner M1 had a peak sound power attenuation of 11.7 decibels, or 46.8 decibels per unit L/D. Although the attenuations at the lower speeds were much lower because of

the lack of MPT's, the BPF attenuations were comparable to those of the BPF liners when put on an equal L/D basis. Liner M2 was much more effective at 4500 rpm at the BPF than liner M1.

The estimated liner impedances for M1 and M2 are shown in figure 3(b) relative to the calculated impedance optimum at 1600 hertz. Although both liners had a lower-than-design resistance. Liner M1 was closest to the impedance optimum. The performance of M1 was even more impressive in view of the lower-than-planned resistance.

Variation of Liner Resistance

This series of tests was conducted to see if the so-called optimum liner (B3) did indeed have the optimum resistance. A liner with less resistance (B4) and a liner with more resistance (B5) were tested and compared with liner B3. All three had about the same reactance.

The directivity of the BPF suppression for the three liners is shown in figure 23. As judged by liner

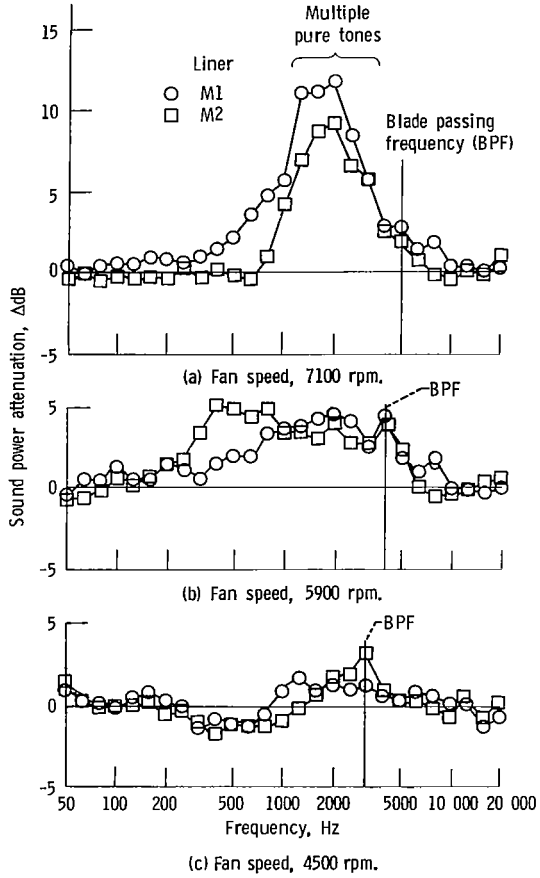

Figure 22. - Sound power attenuation for multiple-pure-tone liners. Length-diameter ratio, 0.25.

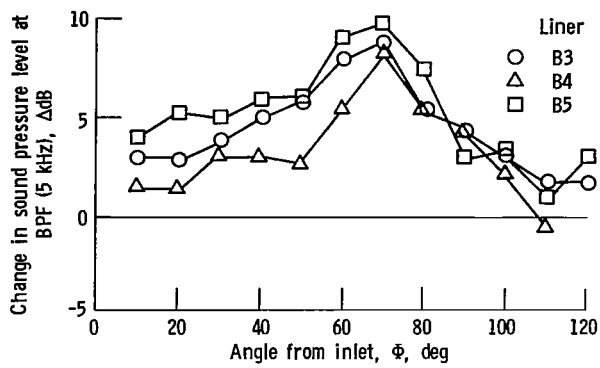

Figure 23. - Effect of liner resistance on blade-passing-frequency suppression for individual liners B3, B4, and B5. Fan speed, 7100 rpm; length-diameter ratio, 0.5.

performance, B5 turned out to be the one closest to being critically damped. Liner B5 had higher attenuations not only at high angles (above 60°), corresponding to the near-cutoff modes for which it was designed, but also at low angles. When the liner properties were evaluated by using measured flow conditions and an updated acoustic resistance model, the test results were understandable. As mentioned in the section Acoustic Liner Design, the original design neglected the effect of boundary-layer thickness on the resistance of the perforated liner wall. This effect was large for the thick boundary layer over these liners. Figure 3(a) shows the recalculated liner impedances for B3, B4, and B5 relative to the optimum. Here, all three liners had a resistance well below the optimum. From this it could be concluded that even liner B5 would benefit substantially from an increase in wall resistance. Liner B4, with the lowest resistance and thus furthest from optimum, showed the poorest performance. The performance of B3 fell between that of B5 and B4, as would be expected from figure 3(a). Unfortunately, none of the liners were overdamped or even critically damped. Thus, the effect of liner acoustic resistance could not be fully determined.

The effect of liner resistance on sound power attenuation at various speeds is shown in figure 24. At 7100 rpm, liner B5 performed better at all frequencies, from the BPF up. The other two liners had almost the same attenuation spectra. At the lower speeds, liners B3 and B5 gave about equal performance at most frequencies, and liner B4 had generally lower attenuation.

Uniform Liner

Instead of two or three different liners being used in an inlet, each designed to remove a different range of modes, a single liner design or uniform liner might

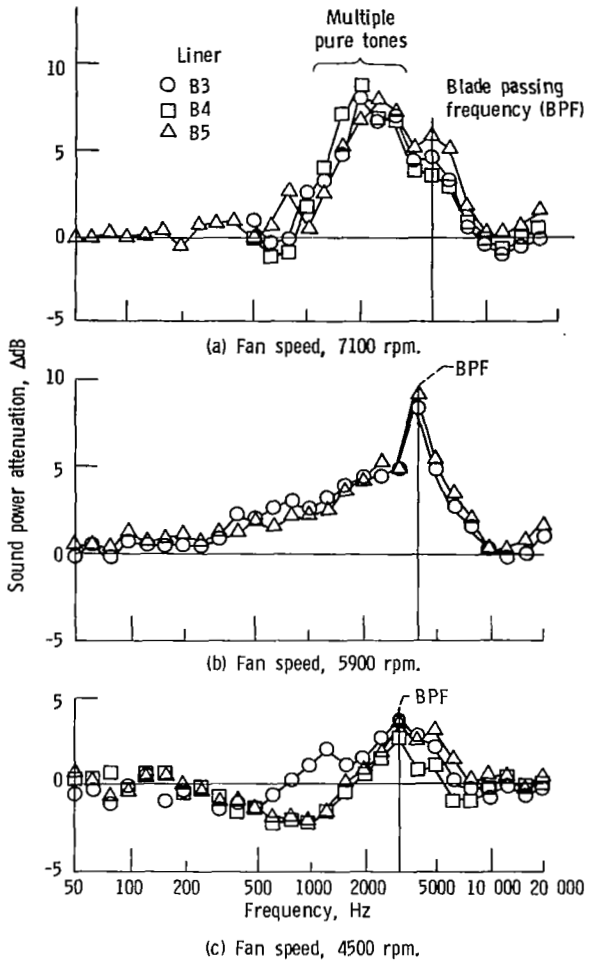

Figure 24. - Effect of liner resistance on sound for individual liners B3, B4, and B5 power attenuation. Length-diameter ratio, 0.5.

be used. The acoustic impedance of this uniform liner should be chosen so as not to be too far from the optimum for any of the modes present. The actual location of this liner impedance relative to the impedance optimum is shown in figure 3(a). Two sections of uniform liner were tested and compared with the liner combination B3 + B2. The active length of the uniform liner was varied by untaping first one-half of a full section, then a full section, and finally two sections for the following length-diameter ratios: 0.25, 0.5, and 1.0. Some of the results for the uniform liner are shown in figure 25, where the directivities of the BPF tone and the tone suppression are plotted. A maximum tone suppression of 14 decibels, as shown in figure 25(b) at a L/D of 1.0, was measured for microphone angles of 60° and 70°. The suppression of these near-cutoff modes was more ef-

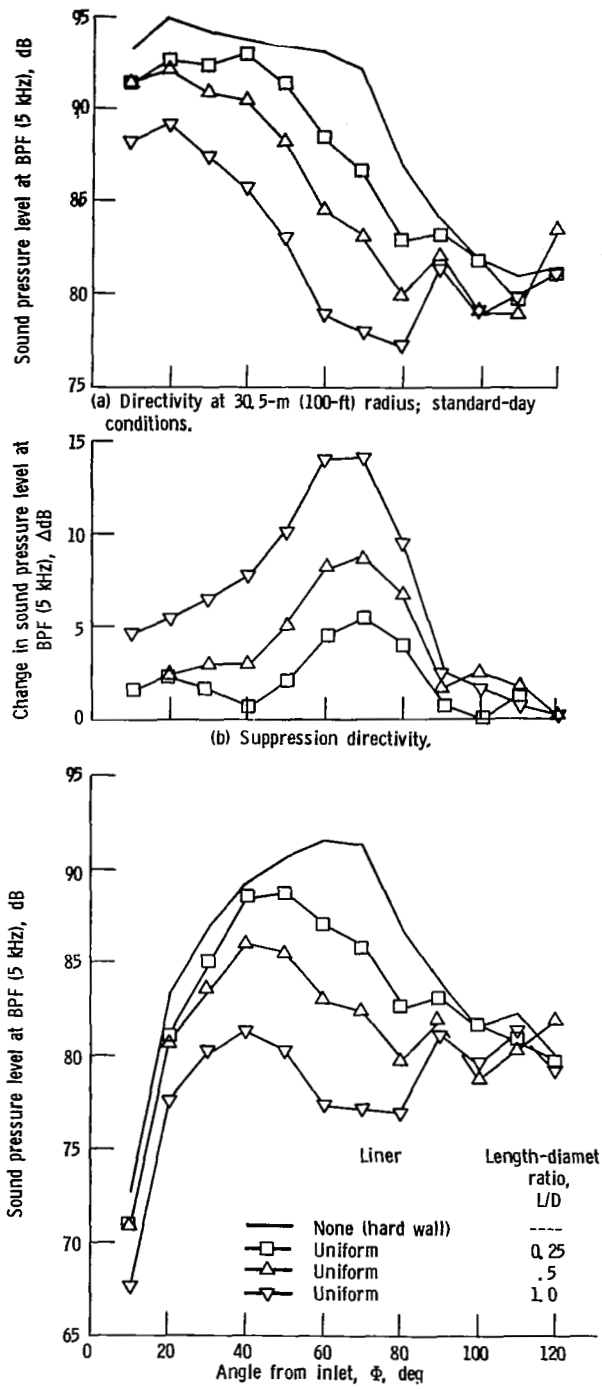

Figure 25. - Blade-passing-frequency performance for variou active lengths of uniform liner. Fan speed, 7100 rpm.

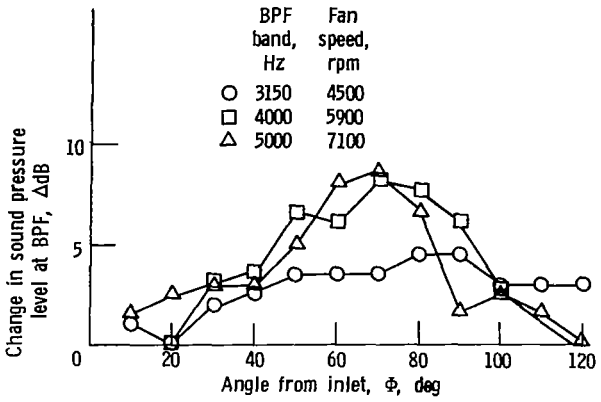

Figure 26. - Effect of fan speed on blade-passing-frequency suppression of uniform liner. Length-diameter ratio, 0.5.

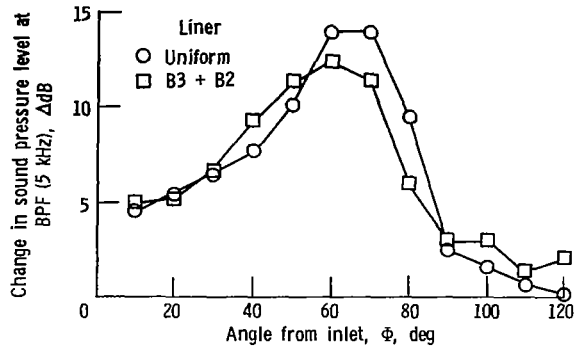

Figure 27. - Blade-passing-frequency suppression for uniform liner and B3 + B2 combination. Fan speed, 7100 rpm; length-diameter ratio, 1.0.

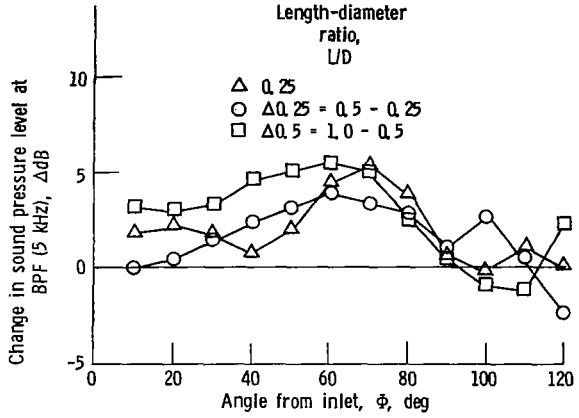

Figure 28. - Incremental blade-passage-frequency suppression for uniform liner at length-diameter ratios of 0.25, 0.5, and 1.0. Fan speed, 7100 rpm.

fective on a sideline basis than was necessary, as shown by the dip in the curve between 60° and 80°. Each curve in figure 25(b) represents a doubling of active length. In most cases the suppression levels were double or less. In those cases where the suppression more than doubled, the initial suppression was usually below 3 decibels and data accuracy might have caused the apparent larger increase. The effect of fan speed on the BPF suppression of the uniform liner with an L/D of 0.5 is plotted in figure 26. The performances at the two highest speeds were similar, but at the lowest speed there was a considerable loss of suppression. This was the only liner that did not have its highest BPF suppression at 5900 rpm.

The uniform liner is compared with multimodal liners in figure 27. Here the B3 + B2 liner combination is compared with two sections of the uniform liner at 7100 rpm. Although the B3 + B2 liner performed slightly better at 40° and 50°, the uniform liner did better at 60° and 80°. Since the differences between the two systems are small, it would appear that either one could be effectively used to suppress the BPF tone.

The incremental change in BPF suppression due to the increase of L/D from 0.25 to 0.5 and finally to 1.0 for the uniform liner is shown in figure 28. The peak BPF suppression for an L/D of 0.25 occurred at 70°. When the liner length was doubled, the peak incremental suppression occurred at 60°, or 10° forward of the original length. Another doubling of length resulted in no change in the angle of the peak incremental suppression. It is interesting to compare this figure with figure 12 for the multimodal liner combinations. The additional suppression attained when liner B2 was added to B3 peaked at 50°, while the additional suppression with the second section of uniform liner peaked at 60°, with higher suppressions than liner B2 from 60° to 90°. One objective of the multimodal liner experiment was to progressively remove more energy from the lower angles, the morecuton modes, as each liner section was added. An indication that this may have occurred is that the peak in the incremental suppression occurred at a lower angle for the second section of the multimodal liner than for the uniform liner.

The sound power attenuation spectra at 7100 rpm for three different active lengths of uniform liner is shown in figure 29. As with other liners at this speed, the MPT's dominated the attenuation spectra. Substantial attenuation was attained at the BPF, with the attenuation almost doubling with each doubling of liner active length. There was a rapid decrease in attenuation above 6300 hertz, as with most of the other liners.

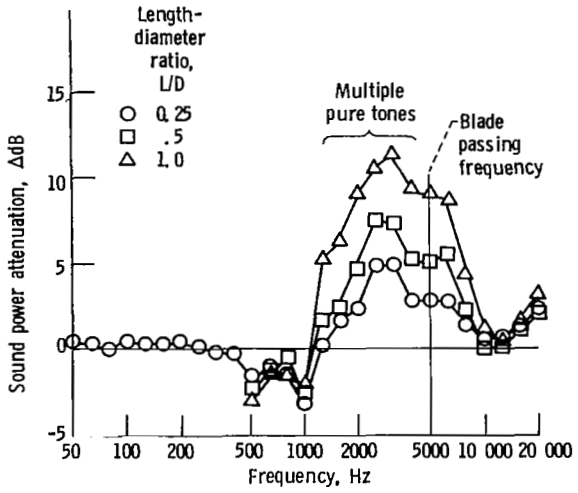

Figure 29. - Sound power attenuation for various active lengths of uniform liner. Fan speed, 7100 rpm.

The effect of fan speed on the sound power attenuation spectrum is shown in figure 30, for one section of liner. The three speed curves generally showed increasing attenuation with speed. As might be expected, the highest attenuations occurred at the MPT frequencies at 7100 rpm.

Progressive Untaping of Liners B3, B5, and B1

This test is similar to the first test discussed, with the liners being untaped in the following order: first B3, designed for near-cutoff modes; then B5, with a higher resistance and also designed for near-cutoff modes; and finally B1, designed for well-cuton modes. The objective here was to try a combination of liners that might be more effective than the original B3 + B2 + B1 combination. Some of the results for this liner combination are shown in figure 31. Here the directivity of the BPF tone and its suppression are plotted for all three stages of untaping. The test of liner B3 alone was a repeat of a previous test and showed very nearly the same results as in figure 11, with a peak suppression at 70°. When liner B5 was made active, there was a substantial increase in suppression. At angles between 20° and 60° the suppression increased by a factor of 2 or more. These large increases in suppression were not completely unexpected since liner B5 had the highest BPF suppression of any of the individual liners tested. Liner B1 was added to yield a small additional increase in suppression. This liner combination gave an increase in peak BPF suppression of 2.4 decibels over the B3 + B2 + B1 combination. As shown in figure 32 the system with liner B5 had higher suppression for all angles in the front quadrant. This suggested an advantage in designing a high percentage of the treatment in an inlet for the near-cutoff modes, at least for a ground static test with all possible propagating modes present.

The effect of fan speed on the BPF suppression of the B3 + B5 + B1 liner combination is shown in figure 33. At 5900 rpm there was a large increase in suppression over that at 7100 rpm. The peak suppression of the BPF was over 21 decibels at an angle of 60°. As with most of the other liners and liner combinations, data at 5900 rpm showed the highest suppression.

To show what each liner section contributed to the total BPF suppression, the incremental suppression due to the addition of each liner was plotted for 7100 rpm in figure 34. When liner B5 was made active, it contributed a large additional suppression with a peak at 60°, or 10° forward of that of liner B3. As noted earlier, at many angles liner B5 added more suppression than liner B3 even though it was the second liner added to the system. Liner B1's contribution was less than that of the other liners. The peak suppression for B1 occurred at 40°, considerably forward of the others. This behavior was consistent with the design objective for this liner (i.e., to remove the well-cuton modes). Liner B1 made a larger contribution to the total BPF suppression of this liner combination than to that of the B3 + B2 + B1 combination (fig. 12). Some of this increase in B1 performance may have been due to there being slightly more energy left in the well cuton modes (angles up to 50°) with the B3 + B5 combination than with B3 + B2. This apparent change in B1 performance may also be an indication of modal scattering.

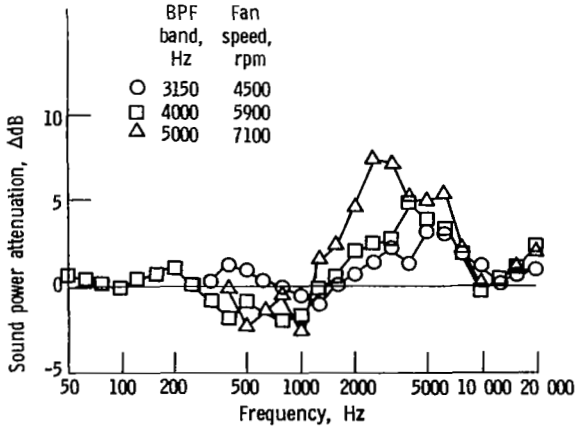

Figure 30. - Effect of fan speed on sound power attenuation for uniform liner. Length-diameter ratio, 0.5.

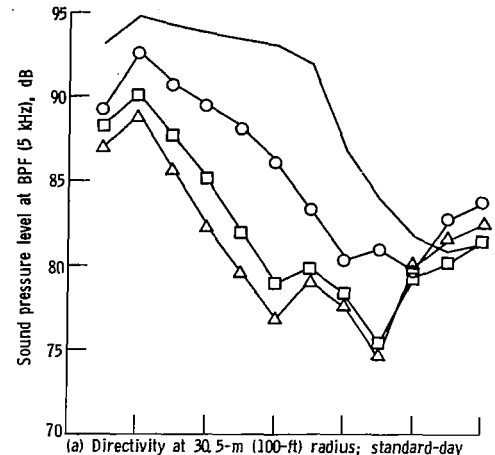

(a) Directivity at 30.5-m (100-ft) radius; standard-day conditions.

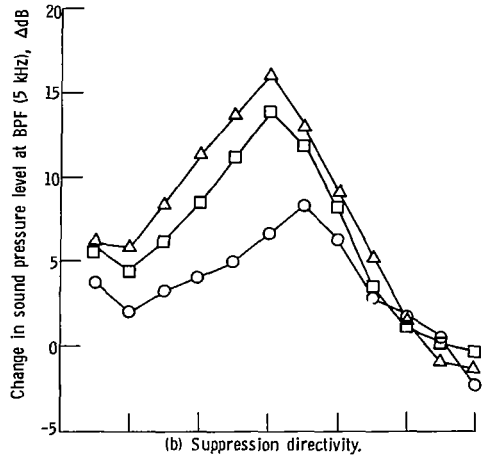

(b) Suppression directivity.

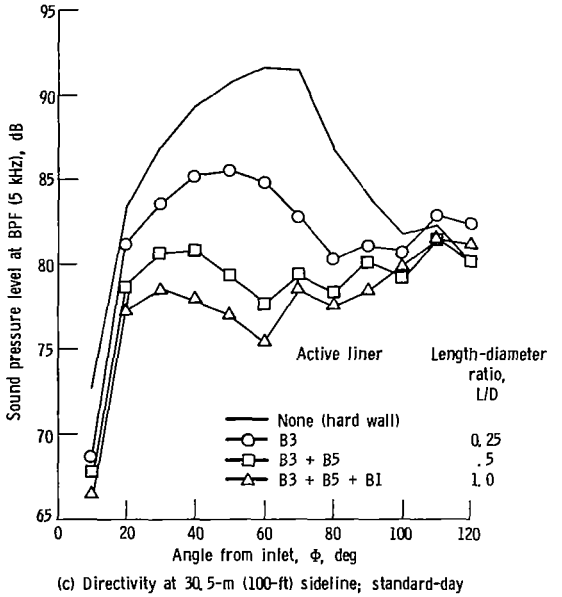

(c) Directivity at 30.5-m (100-ft) sideline; standard-day conditions.

Figure 31. - Blade-passing-frequency directivity and suppression for progressive untaping of liners B3, B5, and B1. Fan speed, 7100 rpm.

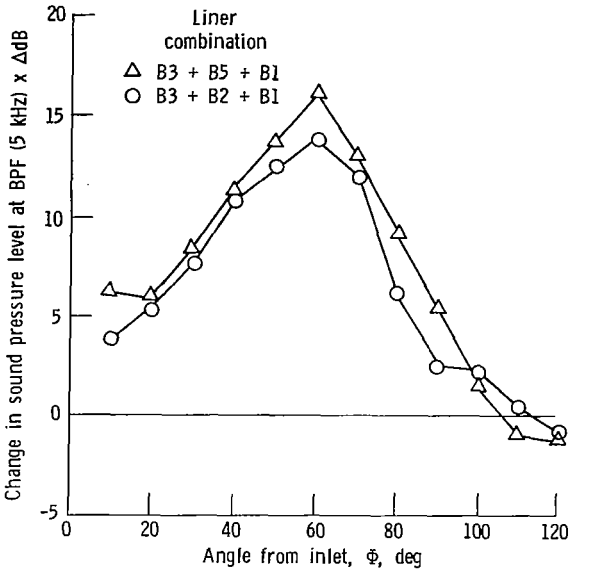

Figure 32. - Comparison of two liner combinations, B3 + B5 + B1 and B3 + B2 + B1. Fan speed, 7100 rpm; length-diameter ratio, 1.5.

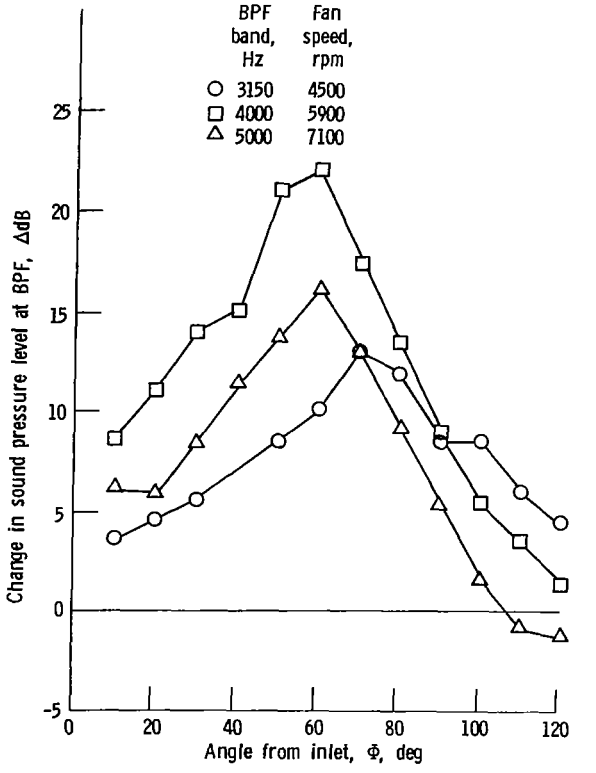

Figure 33. - Effect of fan speed on blade-passing-frequency (BPF) suppression for B3 + B5 + B1 liner combination.

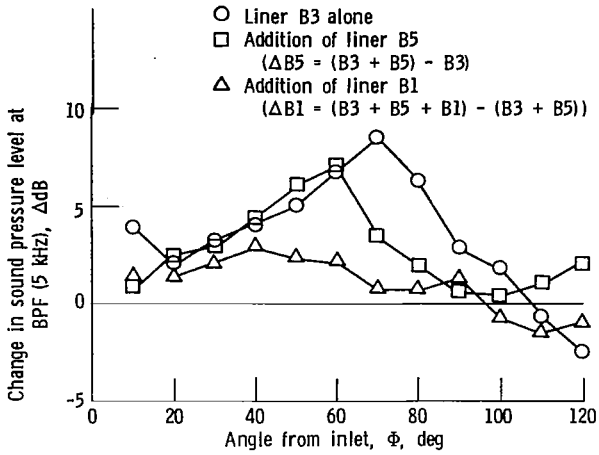

Figure 34. - Incremental blade-passing-frequency suppression for liner combination B3 + B5 + B1. Fan speed, 7100 rpm.

The sound power attenuation spectra for the three stages of untaping of this liner system at 7100 rpm are shown in figure 35. The attenuations of liner B3 were very similar to those in the previous test of this liner. As with all liners tested at 7100 rpm, the MPT's dominated the attenuation spectrum. When liner B5 was added, large increases in attenuation were attained at the MPT and BPF frequencies. At frequencies above the BPF there was a rapid decrease in attenuation to near zero at 10 000 hertz. When the final section of liner (B1) was added, only small increases in attenuation were attained at low frequencies. Larger increases were attained at and above the BPF. Liner B1 gave 3.5 decibels suppression at 10 000 hertz, but the other two liners did not provide any suppression at this frequency. The better high-frequency performance of liner B1 was likely a result of the smaller thickness of this liner. This may have put it closer to optimum impedance for the near-cutoff modes at frequencies higher than the BPF (5000 Hz).

The effect of fan speed on the sound power attenuation spectrum of the full three-liner system is shown in figure 36. At 7100 rpm the easily attenuated MPT's dominated the spectrum between 1000 and 4000 hertz. Above the design frequency (5000) there was a rapid decrease in attenuation, with the liners showing the same performance at the two higher fan speeds. The BPF attenuation at 5900 rpm was almost 16 decibels, the highest attenuation for the three speeds tested. As previously suggested, the high level of attenuation at 5900 rpm was likely a result of a noise source change (i.e., modal power distribution) rather than a liner property. The attenuations at 4500 rpm were generally much lower for all frequencies.

Variation of Boundary-Layer Thickness on Liner B1

Theory shows that the optimum impedance for a liner that is designed for the well-cuton modes is sensitive to the boundary-layer thickness of the inlet flow. This is shown in figure 2, where the three lines representing different boundary-layer thicknesses diverge as the lobe number is decreased (more cuton). Since liner B1 should be the most sensitive to the

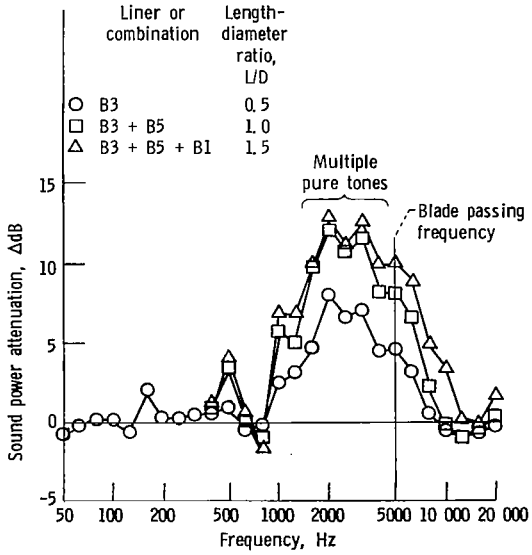

Figure 35. - Sound power attenuation spectra for liner combination B3 + B5 + B1. Fan speed, 7100 rpm.

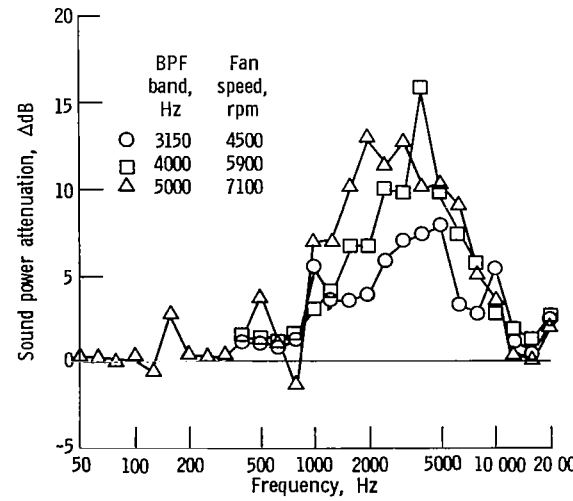

Figure 36. - Effect of fan speed on sound power attenuation for liner combination B3 + B5 + B1. Length-diameter ratio, 1.5.

boundary-layer thickness, it was tested with both thicker- and thinner-than-normal boundary layers. The thinner boundary layer was obtained by using a bleed section just in front of liner B1, as shown in figure 5. The thicker boundary layer was obtained by moving liner B1 downstream, closer to the fan.

For tests where boundary-layer suction was used, baseline (hard wall) noise data were first obtained with the same bleed flow rate as when the liner was active (soft wall). This procedure was necessary for the following reasons: (1) The bleed section provided some suppression of fan noise as soon as it was untaped; (2) the variation of boundary-layer thickness at the fan inlet could cause source noise changes. Noise levels at the BPF were generally 2 to 5 decibels lower when the bleed section was untaped. There was a tendency for the noise to decrease with increasing bleed flow rate. Another problem with data taken when the ejector was operating was that ejector noise interfered with inlet noise measurements. This did not impose any serious limitations on the data. Possible interference with the BPF occurred only at 4500 rpm and at angles of 70° or greater. These data were included in the plots but should be suspect.

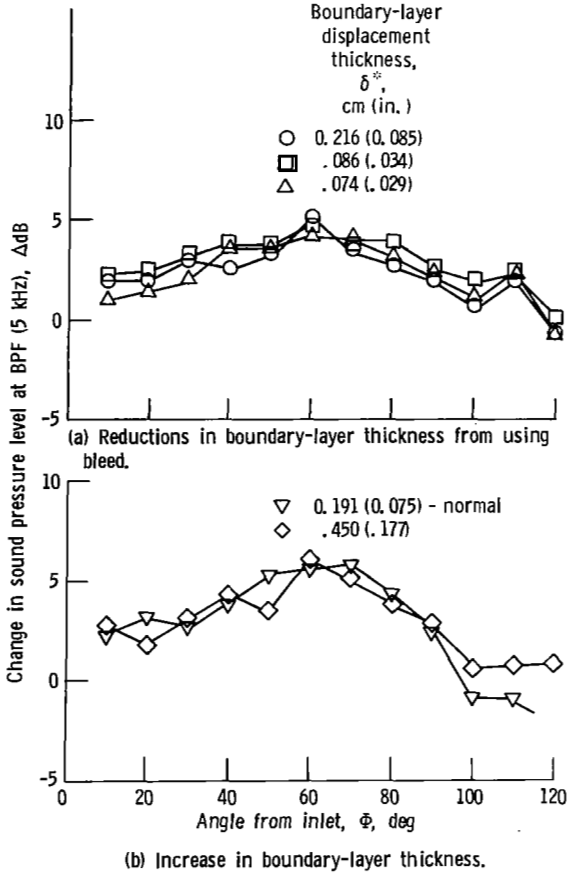

(b) Increase in boundary-layer thickness.

Figure 37. - Effect of boundary-layer thickness on blade-passage-frequency suppression of liner B1. Fan speed, 7100 rpm.

Not until after this test was run was it learned that the boundary-layer thickness not only affected the optimum resistance, but also had a more significant effect than was expected on liner resistance. Originally the boundary-layer thickness effect on liner resistance was thought to be small. This complicated the experiment and is discussed later, after the data are presented.

The effect of boundary-layer thickness on the BPF suppression of liner B1 for the design speed is shown in figure 37. The measured displacement thickness δ was 0.191 centimeter (0.075 in.) for liner B1 in its normal forward position, without bleed. Figure 37(a) shows the effect of lowering δ^* from near normal values to 0.074 centimeter (0.029 in.). No trends were evident over the range of boundary-layer reductions tested. When the boundary-layer thickness was increased (fig. 37(b)), there were again no trends evident in the data. The boundary-layer thickness was varied over a range of almost 6 to 1 with no significant change in the BPF suppression. The BPF suppression at the lower fan speeds for reductions in boundary-layer thickness is shown in figure 38. The only change with boundary-layer thickness that was outside of the data scatter occurred at the minimum thickness (maximum bleed) at 4500 rpm. The data at 10° for the lowest fan speed were erratic and should be suspect. Nevertheless, there seems to be a trend toward higher suppression for the very thin boundary layer. The minimum boundary-layer thickness was limited by the maximum bleed flow rate that could be obtained. For this reason, at the lowest fan speed the greatest fraction of the total inlet flow was removed and the largest boundary-layer reduction was attained. If a δ^* of 0.041 centimeter (0.016 in.) could have been attained at the higher speeds, it is possible that some change in suppression of the liner would have been measured.

The variation of impedance optimum with boundary-layer thickness for the BPF at 7100 rpm is shown in figure 39. The estimated impedance for liner B1 was also plotted for the three boundary-layer thicknesses. These three thicknesses corresponded to the maximum, the normal, and the minimum boundary-layer thicknesses that could be obtained at a fan speed of 7100 rpm. Both the impedance optimum and the B1 actual impedance moved to higher resistances as the boundary layer was reduced. For liner B1, the resistance change with boundary-layer thickness was smaller than the resistance change of the impedance optimum. This difference in the rate of change of resistance was greatest for thin boundary layers. Both the normal and thick boundary-layer impedance for B1 were about the same distance from their corresponding optimum curves. Thus, the

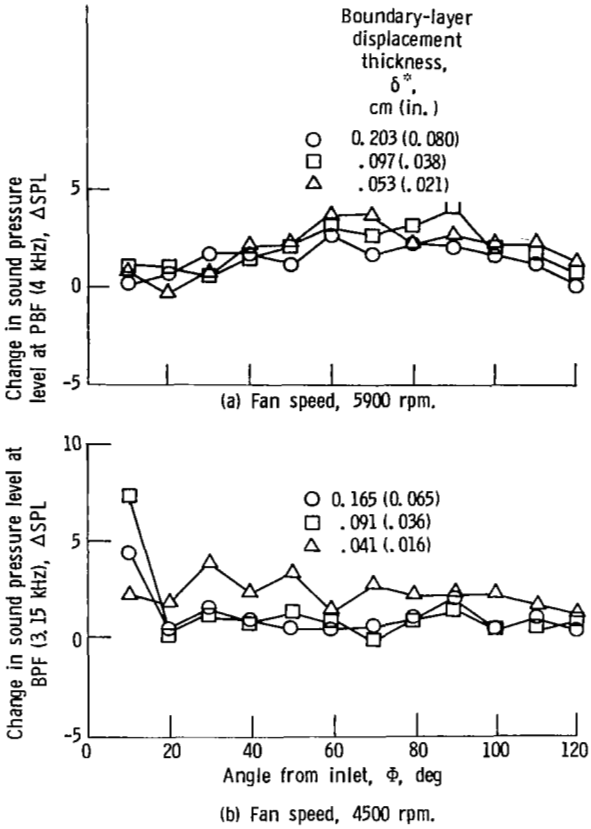

Figure 38. - Blade-passing-frequency suppression for boundary-layer reductions on liner B1 at lower fan speeds.

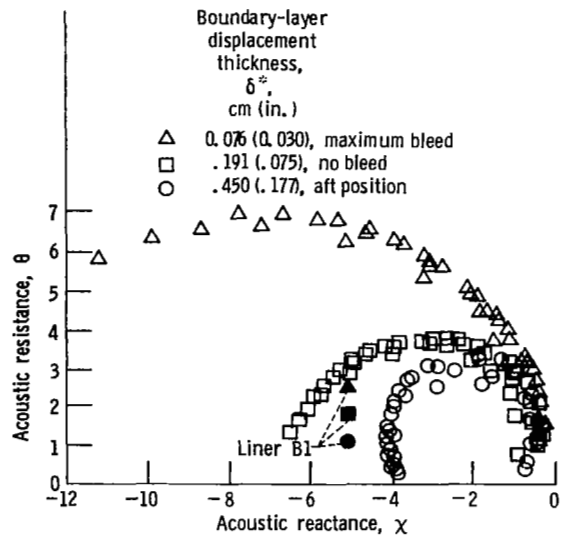

Figure 39. - Impedance optimums and liner B1 impedance for several boundary-layer thicknesses at blade-passing frequency (4733 Hz). Free-stream Mach number, -0.38.

performance for the normal and thick boundary layers would be expected to be the same. This was what was observed. However, when the boundary layer is reduced, there should be a reduction in the attenuation of liner B1. This reduction might be expected to be largest at angles near the axis since it is the well-cuton modes that have the largest change in optimum resistance. This behavior was not observed when the boundary layer was reduced.

One of the factors limiting the experimental ability to measure changes in suppression was the low values of suppression that liner B1 had in the baseline condition. Changes in suppression of at least 1 decibel over several microphone angles should be attained before a trend can be established. With only 2 to 5 decibels of suppression for a baseline, only large-percentage changes in suppression will be noticed.

Another factor limiting this experiment on the change in suppression due to boundary-layer thickness was the presence of modes near the cutoff. Most of the attenuation in figure 37 was due to the attenuation of these near-cutoff modes, as shown by the peak attenuations occurring at the higher angles from the inlet. This point can be further strengthened by comparing the performance of liner B1 in figure 37 and in figure 12. When the near-cutoff modes were removed by liners B3 and B2, as shown in figure 12, only about 1 decibel of suppression was attained with liner B1 and this was mainly at the smaller inlet angles. With the near-cutoff modes clouding the picture in the present experiment, in retrospect not much attenuation change would be expected with boundary-layer change when using liner B1 alone. As shown in figure 39, the modes near cutoff (right side of optimum locus) were quite insensitive to boundary-layer thickness changes, and these were the modes that provided most of the observed attenuation.

Concluding Remarks

The various liners and liner combinations tested are summarized and compared in table III. Three measures of acoustic suppression are listed: blade-passing-frequency (BPF) sound power attenuation in the front quadrant, maximum perceived-noise-level (PNL) suppression on a 152-meter (500-ft) sideline, and maximum BPF suppression (sound-pressure-level (SPL) reduction). These parameters are listed for all three fan speeds tested. Although the peak BPF suppression provided information similar to

TABLE III - SUMMARY OF LINER PERFORMANCE

Configuration	Length-diameter ratio, L/D	Fan speed, rpm													
		4500	5900	7100	4500		5900		7100		4500		5900		7100	
		BPF sound power attenuation (front quadrant), ΔPWL, ΔdB			Maximum PNL suppression at 152-m (500-ft) sideline, ΔPNL						Peak BPF suppression, ΔSPL					
					ΔPNdB	θ, deg	ΔPNdB	θ, deg	ΔPNdB	θ, deg	ΔdB	θ, deg	ΔdB	θ, deg	ΔdB	θ, deg
B3	0.5	3.8	8.5	5.3	5.2	70	10.5	70	8.3	60	7.6	70	14.5	70	8.7	70
B3+B2	1.0	5.6	11.4	8.2	6.8	70	11.2	↓	11.4	60	9.5	↓	16.0	↓	12.5	60
B3+B2+B1	1.5	5.2	12.5	8.5	6.7	60	11.6	↓	10.2	60	8.9	↓	17.1	↓	13.8	60
B3+B2+B1+M1	1.75	5.4	12.7	10.3	6.2	60	12.3	↓	13.9	60	8.5	↓	18.0	↓	15.0	60
1/2 U	0.25	1.3	1.3	2.8	1.8	90	2.9	70	4.0	60	2.5	70 - 90	4.1	70, 80	5.5	70
U	.5	2.3	4.9	5.0	3.2	80	6.0	70	5.3	70	4.9	80, 90	8.3	70	9.0	70
U + U	1.0	4.5	10.5	8.9	4.8	50	10.6	70	9.3	60	7.2	70	14.7	70	14.2	60, 70
B3	0.5	3.0	7.0	4.7	4.7	80	9.1	60	5.7	70	7.5	80	12.7	60	8.6	70
B3+B5	1.0	6.1	13.8	8.2	7.7	70	14.2	60	9.8	60	11.6	70	21.2	60	14.0	60
B3+B5+B1	1.5	7.0	15.8	10.1	9.7	70	15.8	60	11.2	60	13.0	70	22.1	60	16.2	60
B1	0.5	0.8	5.4	4.2	2.4	70	5.1	40	6.0	60	2.7	60	6.7	40	5.8	70
B2	↓	2.3	5.0	3.8	3.5	60	6.2	70	4.7	60	4.5	60, 80	8.4	70	7.3	70
B4	↓	2.8	5.3	3.6	5.9	70	6.0	60	6.4	70	9.2	70	8.2	60	8.2	60
B5	↓	3.6	9.2	5.9	4.7	70	10.6	70	7.2	70	7.8	80	14.6	70	9.5	70
M1, BPF	0.25	1.3	4.4	2.8	3.8	80	5.8	70	6.1	80	6.1	80	6.0	80	4.6	80
M1, 2 kHz, MPT	↓	1.4	4.5	11.7	---	--	----	--	----	--	3.1	60	7.7	70	16.4	70
M2, BPF	↓	3.2	4.0	1.9	4.4	80	5.8	80	5.0	60	8.0	80	7.6	80	3.5	70
M2, 2 kHz, MPT	↓	1.7	4.0	9.2	---	--	----	--	----	--	3.1	60	6.6	60	12.1	60, 80

that in the bulk of the figures previously presented, the BPF sound power attenuation provided an integration of these SPL reductions over the front quadrant. The PNL suppression provided an integration of the SPL reductions over a range of frequencies in an effort to measure annoyance. The PNL suppression reported here was at a fixed angle on the sideline. The liners tested were not designed specifically to lower the PNL, and a liner optimized for PNL suppression would probably attain larger noise reductions. The boundary-layer configurations were omitted from the table because they showed little change from liner B1 results.

The progressive untaping of the B3 + B2 + B1 liner combination shows the difficulty of removing the well-cuton modes. Each liner added was designed to remove progressively more-cuton modes. As each liner was made active, the increase in suppression was considerably less than that of the previous liner. Although there is normally a tendency for added liners to remove progressively less energy, as shown in the table by the uniform liner test, the tendency for the B3 + B2 + B1 combination was larger.

Comparing liner combinations with a length-diameter ratio (L/D) of 1.0 at 7100 rpm shows that the uniform liner was effective in terms of power attenuation and peak BPF suppression. The largest PNL reduction was attained with the B3 + B2 combination despite the fact that it had the lowest peak BPF suppression. The PNL suppression at 7100 rpm in many cases was influenced by the MPT's. The repeatability of the MPT's from day to day was not as good as that of the tones at other frequencies. This might be a result of using physical fan speed instead of corrected fan speed. At 5900 rpm the best liner combination with an L/D of 1.0 was B3 + B5. This combination had impressive performance in terms of all the suppression measurements listed. Comparing combinations with an L/D of 1.5 showed that B3 + B5 + B1 combination did better than B3 + B2 + B1 for all listed suppressions and at all speeds. The general trend seems to be that liner combinations that have the bulk of their treatment designed for the near cutoff modes are the most effective.

Comparing the individual BPF liners shows that liner B5 was the most effective for almost all speeds and suppression measurements. Increasing the liner resistance from B4 to B3 and finally to B5 generally increased the performance at all speeds. An excep-

tion was liner B3 at 7100 rpm, which had more PNL suppression than liner B5. This difference in PNL suppression seems to be a result of MPT suppression differences.

The trend toward higher suppression with liners designed closer to the cutoff was also shown by comparing the individual liners B1, B2, and B3. Liner B2 broke with this trend for the sound power attenuation and PNL suppression for the two higher speeds, although the peak BPF suppression showed the expected progression. The performance of liner B2 was unexpectedly poor, especially when compared with the performance of the uniform liner. The acoustic impedances for liner B2 and the uniform liner were close, and their performances should be similar. No satisfying reason for the poor performance of B2 can be given at this time.

Comparing the two MPT liners at design speed (7100 rpm) showed that the liner M1 was superior in all respects. Here again, the design for the near-cutoff modes performed better than one for the more-cuton modes. This is not surprising in the case of MPT's since most of the energy in the far-field is at high angles from the axis, corresponding to near cutoff. The suppression value for 2000 hertz (typical MPT frequency) was very impressive especially in view of the L/D of 0.25. The PNL suppression for M1 was comparable to that of most of the individual BPF liners even though M1 was one-half as long. Even the BPF suppression was similar to that of the BPF liner when put on the same L/D basis.

The table shows that almost all the liners and liner combinations had better BPF performance at a fan speed of 5900 rpm than at any other speed. As discussed earlier, this behavior seems to be related to the modal energy distribution of the fan noise at this speed (sonic rotor relative tip Mach number) rather than to the liners acoustic properties.

In most cases the changes in the BPF directivity observed were consistent with the theory used in the liner design. For example, as liners designed for progressively more-cuton modes were added to a liner combination, their peak BPF suppression occurred closer to the axis. Although this trend of peak suppression to move toward the axis existed even when liners of the same design (uniform) were added together, it was larger when the liners where designed for progressively more-cuton modes. Liners designed for the near-cutoff modes were generally more effective than ones designed for the more-cuton modes. This was expected since theoretical results indicate that the near-cutoff modes have a higher potential for suppression and that there are potentially a greater number of them present.

Most of the trends and observations of the test data were consistent with the theories and assumptions on which the design philosophy was based. This lends much qualitative support to a design method based on the mode cutoff ratio. Although this design method is presently incomplete, it appears to be headed in the right direction.

There were also results that were not consistent with design theory. For example, in some cases, liners designed for the well-cuton modes were less effective at these modes, based on far-field data, than liners designed for the near-cutoff modes. It was felt that modal scattering resulting from abrupt wall impedance changes may have been complicating the interpretation of these and much of the other data. If this was the case, any complete design method would probably have to include modal scattering effects.

Because the effect of boundary-layer thickness on resistance was neglected in designing the liners, all the liners had significantly lower resistances than planned. Many of the test results would have been more conclusive if the liner resistances were higher (i.e., closer to the design values). These lower-than-planned acoustic resistances also imply that still higher attenuations than obtained here are possible. Thus, the performances of liners like B5 with 19 decibels suppression per unit L/D and M1 with 65.6 decibels suppression per unit L/D may be only part of the maximum attenuation values possible.

The data reported herein could lead to a much better understanding of liner behavior as future analytical advances are made in spinning-mode propagation and attenuation.

Lewis Research Center,
National Aeronautics and Space Administration,
Cleveland, Ohio, September 28, 1979,
505-03.

References

1. Yurkovich, R.: Attenuation of Acoustic Modes in Circular and Annular Ducts in the Presence of Uniform Flow. AIAA Paper 74-552, June 1974.
2. Rice, Edward J.: Spinning Mode Sound Propagation in Ducts with Acoustic Treatment. NASA TN D-7913, 1975.
3. Motsinger, R. E.; Kraft, R. E.; and Zwick, J. W.: Design of Optimum Acoustic Treatment for Rectangular Ducts with Flow. ASME Paper 76-GT-113, Mar. 1976.
4. Rice, E. J.: Inlet Noise Suppressor Design Method Based upon the Distribution of Acoustic Power with Mode Cut-Off Ratio. Advances in Engineering Science, Vol. 3, NASA CP-2001, Vol. 3, 1976, pp. 883-894.
5. Rice, E. J.: Multimodal Far-Field Acoustic Radiation Pattern Using Mode Cutoff Ratio. AIAA J., vol. 16, no. 9, Sept. 1978, pp. 906-911.
6. Rice, E. J.: Acoustic Liner Optimum Impedance for the Spinning Modes with Cut-Off Ratio as the Design Criterion. AIAA Paper 76-516, July 1976. (Also NASA TM X-73411, 1976.)
7. Rice, E. J.: Modal Density Function and Number of Propagating Modes in Ducts. NASA TM X-73539, 1976.
8. Rice, E. J.: Optimum Wall Impedance for Spinning Modes – A Correlation with Mode Cutoff Ratio. J. Aircr., vol. 16, no. 5, May 1979, pp. 336-343.
9. Rice, E. J.: Attenuation of Sound in Ducts with Acoustic Treatment – A Generalized Approximate Equation. NASA TM X-71830, 1975.
10. Schlichting, H. (J. Kestin, transl.): Boundary Layer Theory. McGraw-Hill Book Co., Inc., 1955.
11. Rice, E. J.: A Model for the Acoustic Impedance of a Perforated Plate Liner with Multiple Frequency Excitation. NASA TM X-67950, 1971.
12. Rogers, T.; and Hersh, A. S.: Effect of Grazing Flow on Steady-State Resistance of Isolated Square-Edged Orifices. NASA CR-2681, 1976.
13. Groeneweg, J. F.: Current Understanding of Helmholtz Resonator Arrays as Duct Boundary Conditions. Basic Aerodynamic Noise Research, NASA SP-207, 1969, pp. 357-368.
14. Armstrong, D. L.: Acoustic Grazing Flow Impedance Using Waveguide Principles. (D3-8684, Boeing Co.; NASA Contract NAS3-14321.) NASA CR-120848, 1971.
15. Hersh, A. S.; and Walker, B.: Effect of Grazing Flow on the Acoustic Impedance of Helmholtz Resonators Consisting of Single and Clustered Orifices. NASA CR-3177, 1979.
16. Rice, E. J.: A Theoretical Study of the Acoustic Impedance of Orifices in the Presence of a Steady Grazing Flow. NASA TM X-71903, 1976.
17. Stakolich, E. G.: Design of an Air Ejector for Boundary-Layer Bleed of an Acoustically Treated Turbofan Engine Inlet During Ground Testing. NASA TM-78917, 1978.
18. Montegani, F. J.: Some Propulsion System Noise Data Handling Conventions and Computer Programs Used at the Lewis Research Center. NASA TM X-3013, 1974.
19. Heidelberg, L. J.; and Homyak, L.: Full-Scale Engine Tests of Bulk Absorber Acoustic Inlet Treatment. AIAA Paper 79-600. (Also NASA TM-79079, 1979.)
20. Tsui, C. Y.; and Flandro, G. A.: Self-Induced Sound Generation by Flow Over Perforated Duct Liners. J. Sound Vibr., vol. 50, no. 3, Feb. 1977, pp. 315-331.

1. Report No. NASA TP-1613	2. Government Accession No.	3. Recipient's Catalog No.
4. Title and Subtitle EXPERIMENTAL EVALUATION OF A SPINNING-MODE ACOUSTIC-TREATMENT DESIGN CONCEPT FOR AIRCRAFT INLETS		5. Report Date April 1980 6. Performing Organization Code
7. Author(s) Laurence J. Heidelberg, Edward J. Rice, and Leonard Homyak		8. Performing Organization Report No. E-185 10. Work Unit No. 505-03
9. Performing Organization Name and Address National Aeronautics and Space Administration Lewis Research Center Cleveland, Ohio 44135		11. Contract or Grant No. 13. Type of Report and Period Covered Technical Paper
12. Sponsoring Agency Name and Address National Aeronautics and Space Administration Washington, D.C. 20546		14. Sponsoring Agency Code

15. Supplementary Notes

16. Abstract

An aircraft-inlet noise suppressor design method based on mode cutoff ratio was qualitatively checked by testing a series of liners on a YF-102 turbofan engine. Far-field directivity of the blade passing frequency (BPF) was used extensively to evaluate the results. The trends and observations of the test data lend much qualitative support to the design method. The best of the BPF liners attained a suppression at design frequency of 19 dB per unit length-diameter ratio. The best multiple-pure-tone liner attained a remarkable suppression of 65.0 dB per unit length-diameter ratio.

17. Key Words (Suggested by Author(s))	18. Distribution Statement
Acoustic treatment Aircraft inlet noise Spinning modes Noise suppression	Unclassified - unlimited STAR Category 07

19. Security Classif. (of this report)	20. Security Classif. (of this page)	21. No. of Pages	22. Price*
Unclassified	Unclassified	28	A03

* For sale by the National Technical Information Service, Springfield, Virginia 22161

NASA-Langley, 1980